I. Introduction

1.1 Research Motive

Fiber-reinforced polymeric (FRP) composites have been used extensively in the industry, such as sport appliances, lightweight armor and marine structures, due to their low weight and relatively high strength or stiffness. FRP also offer unique advantage over metallic structures, such as resistance to harsh corrosive environment, and electrical or magnetic insulation in transmission. In general, the mechanical behavior of polymeric matrix in FRP is nonlinear and rate-dependent which imply that FRP composites may also exhibit the nonlinearity and rate sensitivity, especially subjected to off-axis and dynamic loading. To fully understand this characteristic of the materials, it is desired to investigate and characterize the nonlinear rate-dependent behavior of composites.

1.2 Paper Review

A number of theoretical models have used to describe the nonlinear behavior of unidirectional fiber reinforced composite materials. There are two general approaches for modeling the nonlinear behavior, i.e. micromechanical approach [1-5] and macro-mechanical approach [6-19]. The micromechanical approach is based on the analysis of the representative volume element (RVE) consisting of elastic fibers with small diameters surrounded by elastic-plastic matrix. Wu and Shephard et al. [1] presented a micromechanical model, a periodic hexagonal array of elastic fibers embedded in an elastic-plastic matrix, to predict the response of metal matrix composite using Finite Element Method. Sun and Vaidya [2] predicted the elastic constants of the composite from a square RVE through the strain energy equivalence principles in conjunction with three-dimensional finite element method. Zhu and Sun [3] investigated three different unit cells, i.e. the square edge-packing, square diagonal-packing and hexagonal-packing arrangement, to generate off-axis stress-strain curves. Instead of inconvenient FEM, a general closed form

elastic-plastic constitutive equation for metal matrix composites was derived by Aboudi [4] based on the micromechanical model and the assumption that the fibers are rectangular and arranged in a doubly periodic array. Sun and Chen [5] developed a simple micromechanical model to describe the elastic-plastic behavior of off-axis unidirectional composites. It should be noted that the models are analytical and confined to 2-D.

In the macro-mechanical approaches, composites are considered as a homogeneous nonlinear elastic or plastic body. Using complementary elastic energy density, Hahn and Tsai [6] formulated a set of stress-strain relations which is capable of describing the nonlinearity just inherent in the longitudinal shear in unidirectional composite lamina. Lin and Hu [7] proposed a nonlinear analytical model by considering the nonlinear in-plane shear behavior of composites with variable shear parameter to account the possible damage onset in individual lamina. Vaziri and Olson et al. [8] developed an orthotropic plasticity model for the prediction of failure strength. Hansen and Blackketter et al. [9] presented an invariant flow rule for anisotropic plasticity using a scalar hardening parameter instead of effective stress-effective plastic strain relation. Sun and Chen [10] proposed a one parameter plastic potential for describing the nonlinearity of composite. The only one parameter a_{66} in their model can be determined by performing simple tension tests on off-axis specimens with different fiber orientations. Ogi and Takeda [11] presented the effect of moisture content on the nonlinear stress-strain behavior of glass fiber composites with this variable orthotropic parameter. Sun and Lau [12] proposed a 3-D constitutive model for unidirectional composites. In their model, the material anisotropic elastic, anisotropic yielding and anisotropic hardening behavior were considered. Ogihara and Kobayashi et al. [13] investigated the mechanical behavior of carbon/epoxy unidirectional and angle-ply laminates with the one parameter plasticity model. Note that, in the above works, the nonlinear behavior of composites was in focus.

The rate effect on the nonlinear behavior of composite materials has been investigated in

past decades. Bodner and Partom [14] developed a set of constitutive equations for elastic-viscoplastic behavior of isotropic materials which require neither a yield criterion nor the distinction between loading and unloading. A modified Bodner and Partom's model with the one-parameter plasticity model was used to describe the viscoplasticity of thermoplastic composites [15]. Yoon and Sun [15] and Gates and Sun [16] adopted one parameter plastic potential in conjunction with the overstress concept to model the elastic/viscoplastic behavior of the unidirectional fiber composites. The strain rate ranges in their analysis are 10^{-6}/s to 10^{-3}/s. Zhu and Sun [17] characterized nonlinear rate-dependent behavior of off-axis composites at three different strain rates and any combination of loading and unloading rates with over stress concept. For composite laminates consisting of plies with different fiber orientations, the stress and strain relations may also exhibit rate sensitivity. Sun and Zhu [18] also incorporated the overstress viscoplasticity model with the laminated plate theory to predict the responses of symmetric balanced laminates at different strain rates. In order to establish the stress and strain relation, it is required to determine the five parameters in the overstress viscoplasticity model as well as to solve a nonlinear ordinary differential equation. The effects of the residual stress and deformation-induced fiber orientation change on the nonlinear behavior were taken into account in their studies. Thiruppukuzhi and Sun [19] characterized the rate dependent behavior of the unidirectional glass/epoxy composites and the woven E-glass fabric using a three parameter viscoplasticity model. The parameters in the viscoplasticity model were determined from the uniaxial tests on off-axis specimens at three strain rates of 10^{-4}/s, 10^{-2}/s and 1/s. With the assistance of finite element method, the three parameters viscoplasticity model was adopted to predict the rate dependent constitutive relation of composite laminates. By performing high strain rate testing on off-axis composite specimens using a Split Hopkinson Pressure Bar, Tsai an Sun [20] demonstrated that the three parameters viscoplaticity model established based on low strain rate tests was suitable for describing high strain responses of composites at strain rate at least up to 700/s.

1.3 Research Approach

In this study, the three parameters viscoplasticity model was employed in conjunction with the laminated plate theory to predict the constitutive relation of composite laminates at various strain rates. The incremental form of stress and plastic strain relation was generated by using the one parameter plastic potential to describe the flow rule. With the introduction of the viscoplasticity model, the explicit form of the rate dependent plastic modulus in the constitutive formulation was expressed in terms of effective stress and effective plastic strain rate. The corresponding parameters in the viscoplasticity model were determined from the off-axis tensile tests proposed by Thiruppukuzhi and Sun [19]. By implementing the constitutive relation as well as the laminated plate theory, the stress and strain curves of the laminates were established analytically without using the finite element method. Tensile tests were conducted on symmetric glass/epoxy and graphite/epoxy composite laminates at 0.0001/s, 0.01/s, and 1/s strain rates and, based on the experimental results, the model predictions were verified. The thermal residual stress was also considered in laminates prediction.

II. Theory and Method

In order to characterize the nonlinear rate dependent behavior of composites, a viscoplasticity model was proposed based on the one parameter plastic potential together with the associated flow rule. With the aid of laminate plate theory, the viscoplasticity model was extended to describe the rate sensitivity of the stress and strain curves of composite laminates.

2.1 Viscoplasticity Model

In plastic yield criteria [21, 22], a yield function for a general material is assumed as

$$\begin{aligned} 2f(\sigma_{ij}) &= a_{11}\sigma_{11}^2 + a_{22}\sigma_{22}^2 + a_{33}\sigma_{33}^2 \\ &\quad + 2a_{12}\sigma_{11}\sigma_{22} + 2a_{13}\sigma_{11}\sigma_{33} + 2a_{23}\sigma_{22}\sigma_{33} \\ &\quad + 2a_{44}\sigma_{23}^2 + 2a_{55}\sigma_{13}^2 + 2a_{66}\sigma_{12}^2 \\ &= k \end{aligned} \tag{2.1}$$

where σ_{ij} are stresses in the principal material directions. The coefficients a_{ij} refer to the amount of anisotropy and can be determined from the experimental data. For isotropic material, this yield function can be reduced to von Mises yield criterion as

$$\begin{aligned} 2f(\sigma_{ij}) &= \frac{1}{3}\left[(\sigma_{11}-\sigma_{22})^2 + (\sigma_{22}-\sigma_{33})^2 + (\sigma_{33}-\sigma_{11})^2\right] \\ &\quad + 2\sigma_{23}^2 + 2\sigma_{13}^2 + 2\sigma_{12}^2 \\ &= k \end{aligned} \tag{2.2}$$

, and a_{ij} have the values

$$\begin{aligned} a_{11} &= a_{22} = a_{33} = 2/3 \\ a_{12} &= a_{13} = a_{23} = -1/3 \\ a_{44} &= a_{55} = a_{66} = 1 \end{aligned} \tag{2.3}$$

The Hill's yield function for orthotropic material is a special case of equation (2.1) with

$$\begin{aligned} a_{12} &= a_{33} - 1/2(a_{11} + a_{22} + a_{33}) \\ a_{13} &= a_{22} - 1/2(a_{11} + a_{22} + a_{33}) \\ a_{23} &= a_{11} - 1/2(a_{11} + a_{22} + a_{33}) \end{aligned} \tag{2.4}$$

If the similar form as equation (2.2) is chosen, the Hill's function can be expressed as

$$
\begin{aligned}
2f(\sigma_{ij}) &= F(\sigma_{11}-\sigma_{22})^2 + G(\sigma_{22}-\sigma_{33})^2 + H(\sigma_{33}-\sigma_{11})^2 \\
&\quad + 2L\sigma_{23}^2 + 2M\sigma_{13}^2 + 2N\sigma_{12}^2 \\
&= k
\end{aligned} \tag{2.5}
$$

where F, G, H, L, M, and N are material constants characterizing the orthotropic yield behavior. It is noted that the yield function given by equations (2.5) implies that: 1. hydrostatic stress does not produce plastic deformation, 2. the plastic body does not show a Bauschinger effect, in other words, the magnitude of the yield stress is the same in tension and compression.

Figure 2.1 is shown the orthotropic lamina located in the principal coordinate system. Following Hill's criterion and assuming that there is no plastic deformation in fiber direction, i.e. $d\varepsilon_{11}^p = 0$ and that a 2-D plane stress state is prevalent on the 1-2 plane for fibrous composite plate, Sun and Chen [10] proposed the one-parameter plastic potential function as

$$
2f = \sigma_{22}^2 + 2a_{66}\sigma_{12}^2 \tag{2.6}
$$

where a_{66} is orthotropic parameter. By using the one parameter plastic potential to describe the associated flow rule, the plastic strain rates are derived as.

$$
\dot{\varepsilon}_{ij}^p = \frac{\partial f}{\partial \sigma_{ij}}\dot{\lambda} \quad \text{or} \quad \begin{Bmatrix} \dot{\varepsilon}_{11}^p \\ \dot{\varepsilon}_{22}^p \\ \dot{\gamma}_{12}^p \end{Bmatrix} = \begin{Bmatrix} 0 \\ \sigma_{22} \\ 2a_{66}\sigma_{12} \end{Bmatrix}\dot{\lambda} \tag{2.7}
$$

where $\dot{\lambda}$ is a proportionality factor.

Define the effective stress as

$$
\bar{\sigma} = \sqrt{3f(\sigma_{ij})} \tag{2.8}
$$

Through the equivalence of the plastic work rate

$$
\dot{W}^P = \sigma_{ij}\dot{\varepsilon}_{ij}^p = 2f\dot{\lambda} = \bar{\sigma}\bar{\dot{\varepsilon}}^p \tag{2.9}
$$

the proportionality factor $\dot{\lambda}$ is given as

$$\dot{\lambda} = \frac{3}{2}\frac{\dot{\bar{\varepsilon}}^p}{\bar{\sigma}} = \frac{3}{2}\left(\frac{\dot{\bar{\varepsilon}}^p}{\dot{\bar{\sigma}}}\right)\left(\frac{\dot{\bar{\sigma}}}{\bar{\sigma}}\right) \tag{2.10}$$

and the effective plastic strain rate is obtained as

$$\dot{\bar{\varepsilon}}^p = \sqrt{\frac{2}{3}\left[\left(\dot{\varepsilon}_{22}^p\right)^2 + \frac{1}{2a_{66}}\left(\dot{\gamma}_{12}^p\right)^2\right]}^{1/2} \tag{2.11}$$

Sun and Chen [10] has shown that the effective stress $\bar{\sigma}$ and the effective plastic strain $\bar{\varepsilon}^p$ can be obtained form the uniaxial tensile stress-strain curve of off-axis coupon specimens. Under monotonic loading, the effective stress and effective plastic strain have these relations with the uniaxial applied stress σ_x and strain ε_x:

$$\bar{\sigma} = h(\theta)\sigma_x \tag{2.12}$$

$$\bar{\varepsilon}^p = \frac{\varepsilon_x^p}{h(\theta)} \tag{2.13}$$

$$\varepsilon_x^p = \varepsilon_x - \frac{\sigma_x}{E_x} \tag{2.14}$$

where $h(\theta)$ is an off-axis parameter defined as

$$h(\theta) = \sqrt{\frac{3}{2}\left[\sin^4\theta + 2a_{66}\sin^2\theta\cos^2\theta\right]}^{1/2} \tag{2.15}$$

The effective stress-effective plastic strain relation should be unique from stress-strain curves at different values of θ. Therefore, the parameter a_{66} in the plastic potential function must be chosen by trial and error such that the effective stress-effective plastic strain curve obtained from the different off-axis angle θ can be collapsed into one single master curve.

From results of off-axis tension tests, it is indicated that for fibrous composites there is no well defined yield point. In fact, the nonlinearity appears in the stress-strain relation gradually. Therefore, a power law with amplitude A and power n

$$\bar{\varepsilon}^p = A\bar{\sigma}^n \tag{2.16}$$

was used to fit the master effective stress-effective plastic strain curve.

For the rate dependent behavior of composite materials, the parameters of power law function at different strain rates may be changed. In this study, the three parameters

viscoplasticity model proposed by Thiruppukuzhi and Sun [19] for modeling the nonlinear rate dependent behavior of unidirectional composite is introduced. The effective stress and effective plastic strain can be rewritten as

$$\bar{\varepsilon}^{p} = \chi\left(\dot{\bar{\varepsilon}}^{p}\right)^{m}\bar{\sigma}^{n} \tag{2.17}$$

with

$$A = \chi\left(\dot{\bar{\varepsilon}}^{p}\right)^{m} \tag{2.18}$$

a strain rate-dependent coefficient. It is noted that the parameters χ and m are material constants determined by performing uniaxial tests on off-axis specimens at different strain rates. The determination of the material constants for glass/epoxy and graphite/epoxy composites will be presented in the later section. By using the relation of power law, then equation (2.10) become

$$\dot{\lambda} = \frac{3}{2}An\bar{\sigma}^{n-2}\dot{\bar{\sigma}} = An\bar{\sigma}^{n-3}\left(\frac{9}{4}\sigma_{22}\dot{\sigma}_{22} + \frac{9}{2}a_{66}\sigma_{12}\dot{\sigma}_{12}\right) \tag{2.19}$$

Substituting equation (2.19) into equation (2.7), the rate form of plastic strains are expressed

$$\begin{Bmatrix}\dot{\varepsilon}_{11}^{p}\\ \dot{\varepsilon}_{22}^{p}\\ \dot{\gamma}_{12}^{p}\end{Bmatrix} = An\bar{\sigma}^{n-3}\begin{bmatrix}0 & 0 & 0\\ 0 & \frac{9}{4}\sigma_{22}^{2} & \frac{9}{2}a_{66}\sigma_{22}\sigma_{12}\\ 0 & \frac{9}{2}a_{66}\sigma_{22}\sigma_{12} & 9a_{66}^{2}\sigma_{12}^{2}\end{bmatrix}\begin{Bmatrix}\dot{\sigma}_{11}\\ \dot{\sigma}_{22}\\ \dot{\sigma}_{12}\end{Bmatrix} = [U]\begin{Bmatrix}\dot{\sigma}_{11}\\ \dot{\sigma}_{22}\\ \dot{\sigma}_{12}\end{Bmatrix} \tag{2.20}$$

The equation (2.20) is indicates the incremental form of stress and plastic strain relation. It is noted that the entries in the [U] matrix depends on the current stress states and the effective plastic strain rate $\dot{\bar{\varepsilon}}^{p}$.

2.2 Constitutive Relations of Unidirectional Composites

In the case of small incremental strains, the total strain rate can be decomposed into an elastic part and a plastic part as

$$\{\dot{\varepsilon}\} = \{\dot{\varepsilon}^{e}\} + \{\dot{\varepsilon}^{p}\} \tag{2.21}$$

The rate form of elastic stress-strain relation is given by

$$\begin{Bmatrix} \dot{\varepsilon}_{11}^{e} \\ \dot{\varepsilon}_{22}^{e} \\ \dot{\gamma}_{12}^{e} \end{Bmatrix} = \begin{bmatrix} S_{11} & S_{12} & 0 \\ S_{12} & S_{22} & 0 \\ 0 & 0 & S_{66} \end{bmatrix} \begin{Bmatrix} \dot{\sigma}_{11} \\ \dot{\sigma}_{22} \\ \dot{\sigma}_{12} \end{Bmatrix} \tag{2.22}$$

where the elastic compliances S_{ij} and the engineering constants are related by the equations [23]

$$\begin{aligned} S_{11} &= \frac{1}{E_1}, \quad S_{22} = \frac{1}{E_2}, \\ S_{12} &= -\frac{\nu_{21}}{E_2} = S_{21} = -\frac{\nu_{12}}{E_1}, \quad S_{66} = \frac{1}{G_{12}} \end{aligned} \tag{2.23}$$

Substitution of equations (2.20) and (2.22) into equation (2.21), we obtain the incremental stress-strain relations in a time interval for the fibrous composite,

$$\begin{Bmatrix} \dot{\varepsilon}_{11} \\ \dot{\varepsilon}_{22} \\ \dot{\gamma}_{12} \end{Bmatrix} = \begin{bmatrix} S_{11} & S_{12} & 0 \\ S_{12} & S_{22} + \frac{9}{4} An\bar{\sigma}^{n-3}\sigma_{22}^{2} & \frac{9}{2} An\bar{\sigma}^{n-3} a_{66}\sigma_{22}\sigma_{12} \\ 0 & \frac{9}{2} An\bar{\sigma}^{n-3} a_{66}\sigma_{22}\sigma_{12} & S_{66} + 9An\bar{\sigma}^{n-3} a_{66}^{2}\sigma_{12}^{2} \end{bmatrix} \begin{Bmatrix} \dot{\sigma}_{11} \\ \dot{\sigma}_{22} \\ \dot{\sigma}_{12} \end{Bmatrix} \tag{2.24}$$

Making use of the stress and strain transformation laws in the arbitrary *x*-*y* coordinate system (Figure 2.1), then

$$\begin{aligned} \begin{Bmatrix} \dot{\varepsilon}_{xx} \\ \dot{\varepsilon}_{yy} \\ \dot{\gamma}_{xy} \end{Bmatrix} &= [T_{\varepsilon}]^{-1} \begin{bmatrix} S_{11} & S_{12} & 0 \\ S_{12} & S_{22} + \frac{9}{4} An\bar{\sigma}^{n-3}\sigma_{22}^{2} & \frac{9}{2} An\bar{\sigma}^{n-3} a_{66}\sigma_{22}\sigma_{12} \\ 0 & \frac{9}{2} An\bar{\sigma}^{n-3} a_{66}\sigma_{22}\sigma_{12} & S_{66} + 9An\bar{\sigma}^{n-3} a_{66}^{2}\sigma_{12}^{2} \end{bmatrix} [T_{\sigma}] \begin{Bmatrix} \dot{\sigma}_{xx} \\ \dot{\sigma}_{yy} \\ \dot{\sigma}_{xy} \end{Bmatrix} \\ &= [\bar{S}^{ep}] \begin{Bmatrix} \dot{\sigma}_{xx} \\ \dot{\sigma}_{yy} \\ \dot{\sigma}_{xy} \end{Bmatrix} \end{aligned} \tag{2.25}$$

where

$$[T_{\varepsilon}] = \begin{bmatrix} \cos^{2}\theta & \sin^{2}\theta & \sin\theta\cos\theta \\ \sin^{2}\theta & \cos^{2}\theta & -\sin\theta\cos\theta \\ -2\sin\theta\cos\theta & 2\sin\theta\cos\theta & \cos^{2}\theta - \sin^{2}\theta \end{bmatrix} \tag{2.26}$$

$$[T_\sigma]=\begin{bmatrix} \cos^2\theta & \sin^2\theta & 2\sin\theta\cos\theta \\ \sin^2\theta & \cos^2\theta & -2\sin\theta\cos\theta \\ -\sin\theta\cos\theta & \sin\theta\cos\theta & \cos^2\theta-\sin^2\theta \end{bmatrix} \tag{2.27}$$

2.3 Numerical Analysis for Off-Axis Composites

The incremental stress-strain relationships in a time interval given by equation (2.25) are nonlinear, as $[\bar{S}^{ep}]$ depends on the current state of stress and current effect plastic strain rate in lamina. The curve-fit stress versus time curve from the experimental data of off-axis tension test is required to be as an input in numerical simulation. An incremental procedure is used to simulate the nonlinear stress-strain relationship in this study.

The flow chart of the numerical analytic procedure for composite lamina is shown in Figure 2.2. All needed material properties are inputted, and the elastic stiffness matrix $[\bar{Q}^e]$ corresponding to the respective off-axis angle is calculated. A polynomial of three order power-law curve shown in Figure 2.3 can be used to fit tensile stress history recorded from the tensile tests and the results were applied in each incremental loop.

We start with the first time increment from the stress-free state. Thus, for the first stress increments $\{\dot{\sigma}\}$, the elastic-plastic compliance matrix $[\bar{S}^{ep}]$ is obtained with zero values of the current stress, and it becomes the elastic compliance matrix. From equation (2.25) the corresponding strain rate $\{\dot{\varepsilon}\}$ is obtained. The increments of stress and calculated strain are accumulated to represent the current stress and current strain, respectively, after the first time increment.

For the second time increment, the current lamina stress (from the previous accumulated stress) can be used to calculate $[\bar{S}^{ep}]$. It is also needed the rate factor A substituted to express the strain rate effect. To calculation of A, the previous stress rate substitutes into equation (2.22) to get the previous elastic strain rate, the previous total strain rate substitutes

into equation (2.21) to get the previous plastic strain rate, and the definition of effective plastic strain rate in equation (2.11) is used to get the current effective plastic strain rate. The amplitude A is obtained by viscoplastic assumption in equation (2.18). This new calculated $\left[\overline{S}^{ep}\right]$ is then used to obtain the corresponding strain rate $\{\dot{\varepsilon}\}$ for the second time increment. Following the process described above, all the information related to the total stress and strain was obtained. If the time increment is taken to be small enough, the converged stress-strain curve can be established.

2.4 The Laminated Plate Theory

By incorporating the incremental form of stress and strain relation given by equation (2.25) with the laminated plate theory, the constitutive relation for composite laminates can be generated. In other words, the resultant force and the corresponding laminate strain can be expressed explicitly. From equation (2.25), the rate form of stress-strain relation for the k_{th} ply become

$$\begin{Bmatrix} \dot{\varepsilon}_{xx} \\ \dot{\varepsilon}_{yy} \\ \dot{\gamma}_{xy} \end{Bmatrix}_k = \left[\overline{S}^{ep}\right]_k \begin{Bmatrix} \dot{\sigma}_{xx} \\ \dot{\sigma}_{yy} \\ \dot{\sigma}_{xy} \end{Bmatrix}_k \tag{2.28}$$

The tensor stresses of plies in terms of tensor strains of plies are given by

$$\begin{Bmatrix} \dot{\sigma}_{xx} \\ \dot{\sigma}_{yy} \\ \dot{\sigma}_{xy} \end{Bmatrix}_k = \left[\overline{S}^{ep}\right]_k^{-1} \begin{Bmatrix} \dot{\varepsilon}_{xx} \\ \dot{\varepsilon}_{yy} \\ \dot{\gamma}_{xy} \end{Bmatrix}_k = \left[\overline{Q}^{ep}\right]_k \begin{Bmatrix} \dot{\varepsilon}_{xx} \\ \dot{\varepsilon}_{yy} \\ \dot{\gamma}_{xy} \end{Bmatrix}_k \tag{2.29}$$

According to laminated plate theory, the strain rate in laminate represent strain rate in all of plies. Therefore, by integrating equation (2.29) through the laminate thickness, we obtain

$$\begin{Bmatrix} \dot{N}_x \\ \dot{N}_y \\ \dot{N}_{xy} \end{Bmatrix} = \sum_k \left[\overline{Q}^{ep}\right] h_k \begin{Bmatrix} \dot{\varepsilon}_{xx} \\ \dot{\varepsilon}_{yy} \\ \dot{\gamma}_{xy} \end{Bmatrix} = [R] \begin{Bmatrix} \dot{\varepsilon}_{xx} \\ \dot{\varepsilon}_{yy} \\ \dot{\gamma}_{xy} \end{Bmatrix} \tag{2.30}$$

and

$$\begin{Bmatrix} \dot{\varepsilon}_{xx} \\ \dot{\varepsilon}_{yy} \\ \dot{\gamma}_{xy} \end{Bmatrix} = [R]^{-1} \begin{Bmatrix} \dot{N}_x \\ \dot{N}_y \\ \dot{N}_{xy} \end{Bmatrix} = [G] \begin{Bmatrix} \dot{N}_x \\ \dot{N}_y \\ \dot{N}_{xy} \end{Bmatrix} \tag{2.31}$$

For the off-axis tension test, $\dot{N}_y = \dot{N}_{xy} = 0$. Then equation (2.31) is reduced to:

$$\dot{\varepsilon}_{xx} = G_{11}\dot{N}_x \tag{2.32}$$

$$\dot{\varepsilon}_{yy} = G_{21}\dot{N}_x \tag{2.33}$$

$$\dot{\gamma}_{xy} = G_{31}\dot{N}_x \tag{2.34}$$

For a given laminate loading rate, the corresponding strain rate in the laminates can be calculated.

2.5 Numerical Analysis for Composite Laminates

The rates of stress and strain in composite laminate panel given by equation (2.31) are nonlinear, and depend on the current stress state and amplitude A in each ply. The accumulative procedure similar to that in section 2.3 is used to simulate the stress-strain relation of laminates.

Figure 2.4 shows the flow chart of the numerical analytic procedure. At first step, material constants (E_1, E_2, ν_{12}, and G_{12}) and parameters (a_{66}, n, χ, and m) are inputted and elastic stiffness matrix $\left[Q^e\right]_k$ in kth ply are calculated. The thermal expansion coefficients (α_1 and α_2) are also inputted. Due to the mismatch of the thermal expansion coefficients for composite laminates containing numbers of plies with different fiber orientations, thermal residual stress in each ply may exist and affect the nonlinear behavior of the laminates. The detailed derivation for the thermal residual stress based on linear thermal-elasticity is presented in Appendix A.

The incremental procedure began from the zero mechanical stress states. However, the thermal residual stresses are present initially and considered as the initial stress state in each ply. At the beginning, arbitrary values of effective plastic strain rate was assumed in each ply to estimate the corresponding amplitude A in the viscoplasticity model. It was found that the initial selection of plastic strain rate in the plies would not affect the stress and strain curves predicted based on the current incremental procedure. The elastic-plastic compliance matrix $\left[\bar{S}^{ep}\right]_k$ is dependent on the initial stress and rate factor A in plies. In the first stress increments, the corresponding laminate strain increments $\{\dot{\varepsilon}\}$ were obtained from equation (2.31), and the strain value can also be interpreted as the strain rate in each ply. With the constitutive equation (2.29), the corresponding stress increments at each ply were evaluated. The incremental of stress-strain of each ply are accumulated to represent the current stress and current strain in each ply, respectively.

In the second time increment, the current stress in each ply (from the previous accumulated stress in each ply) and rate factor A in each ply were needed to calculate $\left[\bar{S}^{ep}\right]$. To calculate the value of A at each ply, the previous stress rate in each ply was substituted into elastic stress-strain relation (equation (2.22)) to obtain the associated elastic strain rate in each ply. Similarly, the previous total laminate strain rate was substituted into equation (2.21) to evaluate the previous plastic strain rate in each ply. Through the definition of effective plastic strain rate given in equation (2.11), the current effective plastic strain rate in each ply was obtained. From the above works, the amplitude A in each ply is calculated using equation (2.18). The new calculated $\left[\bar{S}^{ep}\right]_k$ is integrated to update the matrix [G] in equation (2.31). The matrix [G] was employed for the generation of the stress and strain curves in the current time increment. If every time increment is taken to be sufficiently small, the plotted stress-strain curve of laminate will be the convergence. The numerical codes for example of prediction of $\left[\pm 30\right]_{3s}$ graphite/epoxy laminate are listed in Appendix

B.

It should be noted that the arbitrary value of the effective plastic strain rate is assumed in the first loop. As a result, in the first few stops, the effective plastic strain rates are quite varied as shown in the figure (2.5). However, after few loops, the effective plastic strain rate curves are coincided together. This is cause that in the elastic-plastic compliance $\left[\bar{S}^{ep}\right]_k$, the effects of the effective stress and the effective plastic strain rate are coupled, and in the initial state, the effective stress is quite small which dramatically reduce the influence of the effective plastic strain rate. Thus, the $\left[\bar{S}^{ep}\right]_k$ is not affected by $\bar{\dot{\varepsilon}}^{p}$ in each ply and almost the same with the elastic compliance $\left[\bar{S}\right]_k$.

III. Setup of Experiments

Two material systems, glass/epoxy and graphite/epoxy, were studied in this investigation. For glass/epoxy composite, S2 type of glass fiber and 8552 type of epoxy are provided in the form of prepreg from Hexcel Company USA. For graphite/epoxy composite material, the CFA type prepreg (fiber volume fraction $\nu_f = 0.49$) with Toho HTA graphite fiber (density = $1.76\,{}^{g}\!/\!_{cm^3}$) was provided from Adgroup Taiwan. Twenty-four plies unidirectional glass/epoxy composites and ten plies unidirectional graphite/epoxy composites were laid up manually and then cured with the recommended curing process. For graphite/epoxy material, the curing history of temperature and pressure is shown in Figure 3.1. By following this curing cycle, the fiber volume fraction of graphite/epoxy is raised to 0.54 approximately.

3.1 Experimental Procedure of Tension Tests

In order to determine the strain rate effect on the nonlinear material behavior of composites, the specimens were tested at three different strain rates, 0.0001/s, 0.01/s and 1/s. Basically, the experiments were divided into two parts. The one is the off-axis specimen testing for determining the parameters in the viscoplasticity model. The other is the tests for composite laminates to verify that the viscoplasticity model in conjunction with laminated plate theory is proper for characterizing the rate sensitivity to the nonlinear behavior of laminates.

3.1.1 Experimental Setup

The tension tests were performed in a closed-loop servo-hydraulic MTS 810 testing machine capable with a maximum capacity of 98 KN. The Schematic of tension test and data collection system is shown in Figure 3.2. A stroke control mode was selected for all tests. Three different strain rates 0.0001/s, 0.01/s, and 1/s were set to conduct the tests.

Measured continue force and displacement signal are collected in MTS controller sever and then outputted to data acquisition system. Back-to-back Micro-Measurement EA-13-240LZ-120 strain gages were mounted on the specimen to measure the tensile strain. Adhesive back-to-back gages in the middle of specimens can compensate for the bending effects. With excited voltage 3V from dynamic strain amplifier, the Wheatstone bridge determines the change in resistance which a gage undergoes when it is subjected to a strain. And appropriate multiple to amplify potential difference of bridge can get reduced-noise signal from dynamic strain amplifier. Load, displacement, and strain signals are required using an analog-to-digital signal converter and recorded by using data acquisition system.

3.1.2 Off-Axis Tests

Coupon specimens were prepared from unidirectional glass/epoxy and graphite/epoxy composite panels, which were 1.8 mm and 1.5 mm thick respectively. All specimens are cut with length 150 mm and width 17.8 mm from the composite panels using diamond saw. End tabs made of glass fiber composite were adhered on the two sides at the ends of the specimens. All dimensions of tensile specimen are shown in Figure 3.3.

The material properties, E_1 and E_2, for the composites were determined using coupon specimens with fiber orientations 0° and 90° tested at strain rate 0.0001/s. Tensile specimen performed on the MTS 810 system is shown in Figure 3.4. Vertical back-to-back strain gages were mounted on the 0° specimen to obtain the Poisson ratio ν_{12}. Determination of Shear modulus G_{12} was reached by using vertical back-to-back strain gages on the $[\pm 45]_{3S}$ laminate. The slope of stress-strain curves was obtained under the strain range 0%~0.1% to evaluate material properties. Elastic material properties for two materials were shown in Table 1 and 2, respectively.

For off-axis tests, specimens are cut at angles 15°, 30°, 45°, and 60° with the same dimensions. An oblique end-tab design associated with material properties is proposed by

Sun and Chung [24]. It is used to ensure that the axial stress and strain of coupon specimens were maintained uniform in uniaxial loading. Three coupon specimens for each angle are tested at strain rates of 0.0001/s, 0.01/s, and 1/s respectively. The strain rate was the stroke rate of the loading frame divided by the original specimen gage length. The 15°, 30°, 45°, and 60° off-axis coupon specimens were tested until failure happened to obtain the stress-strain curves at three different strain rates of 0.0001/s, 0.01/s, and 1/s. All the results of off-axis tension test at three different strain rates are showed in Figure 3.5-3.7 for glass/epoxy and Figure 3.8-3.10 for graphite/epoxy material.

3.1.3 Parameter Evaluation

To completely model the rate dependent response of composite, the orthotropic coefficient a_{66} in the plastic potential function and the parameters in the viscoplasticity model need to be determined. For evaluation of the parameter a_{66}, the mater effective stress-effective plastic strain curve is needed. From equations (2.12), (2.13) ,and (2.14), the effective stress-effective plastic strain curves for different fiber orientations 15°, 30°, 45°, and 60° can collapse into a single effective stress-effective plastic strain curve for a certain strain rate by choosing a proper value of a_{66}. The master effective stress-effective plastic strain curve was then fitted by power law. Figure 3.11-3.13 are showed the master curves for glass/epoxy with $a_{66} = 1.6$ at three different strain rates, and the master curves with $a_{66} = 1.4$ for graphite/epoxy are showed in Figure 3.14-3.16. However, from equation (2.17), it has be observed that the amplitude A is a function of the effective plastic strain rate $\dot{\bar{\varepsilon}}^p$ and the power n is constant for all the strain rates considered. By incorporating these three master curves at three different strain rates showed in Figure 3.17 and Figure 3.18, it is obvious that these two composite materials exhibit meaningful rate dependent behavior. From equation (2.18) amplitude A as a function of the effective plastic strain rate can be plotted in Figure 3.19 and 3.20 on a log-log scale for the two material systems. The

parameters χ and m are determined from these plots as the intercept and the slope, respectively. By following above procedures, three parameters n, χ, and m are determined. It is noted that although the parameters in the viscoplasticity model are determined at lower strain rates, they are still valid at strain rate at least up to 700/s [20]. The values of the parameters in the viscoplasticity model together with elastic material constants for glass/epoxy and graphite/epoxy composite are listed in Table 1 and 2.

3.1.4 Tests Results for Composite Laminates

In order to verify that the viscoplasticity model incorporated with the laminated plate theory suitable for characterizing the nonlinear rate-dependent stress and strain curves on the laminates, tensile tests were carried out on the specimens at three strain rates of 0.0001/s, 0.01/s and 1/s. Two composite material systems were investigated in this study. One is glass/epoxy Composites with stacking sequences $[\pm 45/90_2]_{4s}$, $[75_2/-60/30]_{4s}$, and $[60_2/-75/15]_{4s}$. The other is graphite/epoxy composites with stacking sequences $[\pm 45]_{3s}$, $[60/-30]_{3s}$, $[\pm 60]_{3s}$, and $[\pm 30]_{3s}$. It is noted that since the presence of 0 degree fiber in the laminates will significantly reduce the nonlinear behavior, there are no 0 degree plies contained in the laminates. To be consistent, the curing process used for unidirectional composites was employed for the laminates. Coupon specimens with gage length of 100 mm and width of 17.8 mm were cut from the composite panels using diamond saw.

Uniaxial tensile tests were conducted on the specimens using MTS 810 system with three different strain rates. All the experiment results are shown in Figure 3.21-3.27.

3.2 Measurement of Thermal Expansion Coefficients of Composites

For considering thermal residual stress effect on composite laminates, the principal thermal expansion coefficient of unidirectional fiber composite must be measured. Here, a simple measurement method [25] is used by employing strain gages adhered on a composite panel

under temperature variation.

3.2.1 Principle of the Measurement Technique

When an electrical resistance strain gage is installed on a stress-free specimen, and the temperature of material is changed, the thermal output of the gage change correspondingly. But it should not be assumed that the thermal output is linear with temperature, since (a) differences in the coefficients of thermal expansion (CTEs) of the test material, gage backing, and gage-foil alloy and (b) changes in the electrical properties of the gage alloy which occur with a change in temperature. The principle of measuring the CTE, α, consist of installing two identical electrical resistance strain gages onto two stress-free specimens [26]: (1) the test specimen of unidirectional composite, having α unknown; (2) the reference specimen, having α known. If the two specimens are exposed to the same variation of temperature ΔT and the transverse sensitivity $K_t = 0$ is assumed, it can be shown that the CTE of the test specimen relative to the CTE of the reference one can be obtained from the difference of the output of the two strain gages as

$$\alpha_x - \alpha_r = \frac{\varepsilon_x - \varepsilon_r}{\Delta T} \tag{3.1}$$

where x is the direction of installation of the strain gage in the test material, α_x is the CTE of the test specimen along the measurement direction, α_r is the CTE of the reference material, ε_x is the thermal output from the gage in the test specimen and ε_r is the thermal output from the gage in the reference specimen.

The basic circuit arrangement, shown in Figure 3.28, uses the properties of the half-bridge circuit to perform the subtraction electrically. When the two gages are connected as adjacent arms of the bridge circuit, with excited voltage V, the instrument output ΔE is equal to the difference in the individual thermal outputs. The circuit is obviously simple and direct-reading. In adjacent arms of the bridge circuit, it is noted that leadwires connected to

gages should be particularly well-matched and maintained physically together throughout their lengths. It would minimize differential resistance changes which could appear in the instrument output. With a thermal couple placed adjacent to the gage, differences of temperature and strain would be immediately measured.

3.2.2 Correction of the Error from Transverse Sensitivity

In essence, the transverse sensitivity is a measure of the sensitivity of the strain gage to strains acting in the transverse direction of the gage grid. In most applications a strain gage is used to measure strains in the grid direction, and hence a very low transverse sensitivity is usually desirable. As a result, the CTEs of composite between the axial and transverse direction is very different, the CTE in axial direction is much smaller than in transverse direction for graphite-epoxy composite material, thermal output in axial direction would be required to correct due to the error from transverse sensitivity. The relation between the measured thermal output and the true thermal output was shown [27].

In figure 3.29, it is assumed that a strain gage subjected to a biaxial-strain field. The change in gage resistance induced by the biaxial-strain field is given by:

$$\frac{\Delta R}{R} = F_a \varepsilon_a + F_t \varepsilon_t \tag{3.2}$$

where

R= original gage resistance

ε_a =strains in gage grid direction

ε_t =strain transverses to gage grid

F_a =axial-gage factor

F_t =transverse-gage factor

It is noted that the axial-gage factor is not equal to the gage factor, F_g, reported by the manufacturer.

The transverse sensitivity coefficient, K, is defined as

$$K \equiv \frac{F_t}{F_a} \tag{3.3}$$

This coefficient is supplied by the manufacturer with strain-gage package. Then equation (3.3) can be rewritten in terms of K as follow:

$$\frac{\Delta R}{R} = F_a\left(\varepsilon_a + K\varepsilon_t\right) \tag{3.4}$$

During calibration, the gage is mounted to a standard calibration material which $\nu_0 = 0.285$ and subjected to a uniaxial stress loading. The grid direction is parallel to the uniaxial stress. Under these conditions, the transverse strain applied to the gage is due to Poisson effect, and is given by

$$\varepsilon_t = -\nu_0\varepsilon_a \tag{3.5}$$

Equation (3.4) for this loading condition become:

$$\frac{\Delta R}{R} = F_a\left(1-\nu_0 K\right)\varepsilon_a \tag{3.6}$$

The gage factor supplied by the manufacturer is defined as

$$F_g \equiv F_a\left(1-\nu_0 K\right) \tag{3.7}$$

Finally, equation (3.6) can be rearranged as

$$\varepsilon_a = \frac{\left[\frac{\Delta R}{R}\right]}{F_g} \tag{3.8}$$

Equation (3.8) is derived based on the following assumptions: (a) The strain gage is subjected to a uniaxial stress field; (b) The gage grid is parallel to the direction of stress; (c) The gage is mounted on a material whose Poisson's ratio equals ν_0. If a strain gage is used during a test in above three conditions, then the measured strain ε_m is given by equation (3.8) directly.

$$\varepsilon_m = \varepsilon_a = \frac{\left[\frac{\Delta R}{R}\right]}{F_g} \tag{3.9}$$

Under any other conditions, equation (3.8) is not suitable, and appreciable measurement

error can occur due to transverse sensitivity. In these cases the measured strain must be corrected for transverse sensitivity effect. At least two orthogonal strain measurements are required to correct these errors. A biaxial-strain-gage rosette can get two orthogonal measured strains ε_{mx} and ε_{my}, and the true strain ε_x and ε_y are simply given by:

$$\varepsilon_x = \frac{(1-\nu_0 K)(\varepsilon_{mx} - K\varepsilon_{my})}{1-K^2} \tag{3.10}$$

$$\varepsilon_y = \frac{(1-\nu_0 K)(\varepsilon_{my} - K\varepsilon_{mx})}{1-K^2} \tag{3.11}$$

Equations (3.10) and (3.11) would be used in the correction of the error form the measurement of CTE of fiber composites.

3.2.3 Measurement Procedures and Results

Experiments were performed for the measurement of the CTEs α_1 and α_2 of glass/epoxy and graphite/epoxy unidirectional composites by using electrical resistance strain gage rosettes. The test specimens were prepared from previously 10-plied graphite/epoxy and 24-plied glass/epoxy unidirectional composite panels, which was 1.8 mm and 1.5 mm thick respectively. The specimen was cut with dimension 24×48 mm. Micro-Measurements EA-06-062TT-120 rosettes all belonging to the same lot and the same package were used. This type of gage has two perpendicular grids used to determine principal thermal output with various temperatures. The reference material is ultra-low-expansion titanium silicate which is available from Micro-Measurements for the temperature compensation of dummy gages. When the two gages, installing on test specimen and reference material respectively, are connected as adjacent arms of the two bridge circuits, the instrument outputs of axial direction and transverse direction are equal to the difference in their individual thermal outputs. A thermal couple is placed adjacent to the gage installing on test specimen to measure the temperature difference. Test specimen and reference material are put in the programmable-control oven with heating 15°C/hour and free

cooling about 20°C/hour. The most gradual slope of temperature-time will minimize thermal hysteresis effect and residual stress in the specimen. Test specimen must be placed as free suspension to reduce friction force effect on specimen surface (see Figure 3.30). Continuous temperature difference and strain data are read in conjunction with data acquisition system. Figure 3.31-3.34 are shown the measurement results in two principal directions for glass/epoxy and graphite/epoxy composites, respectively. The transverse sensitivity error is corrected in fiber direction for two materials. It is noted that, for graphite/epoxy composite, it has a near zero value of thermal expansion coefficient. Finally, the thermal expansion coefficients fitted from measurement strain data are $\alpha_1 = 7 \times 10^{-6} / °C$ and $\alpha_2 = 18.3 \times 10^{-6} / °C$ for glass/epoxy and $\alpha_1 = 0.57 \times 10^{-6} / °C$ and $\alpha_2 = 41.4 \times 10^{-6} / °C$ for graphite/epoxy respectively.

IV. Results of Prediction and Discussion

4.1 Model Predictions for Off-Axis Composites

By following the analysis presented in chapter 2.3 for off-axis composites, model predictions for glass/epoxy and graphite/epoxy materials at various strain rate compared with uniaxial tensile tests were depicted in Figures 4.1-4.6, respectively together with experimental results. It is obvious that all modeling results at various off-axis angles were good predictions in both linear-elastic and nonlinear parts.

4.2 Model Predictions for Composite laminates

Figure 4.7, 4.8 and 4.9 depict the comparison of experimental stress-strain curves and model predictions for $[\pm 45/90_2]_{4s}$, $[75_2/-60/30]_{4s}$, and $[60_2/-75/15]_{4s}$ glass/epoxy composite laminates at three different strain rates, respectively. The predictions were based on the viscoplasticity model together with the laminated plate theory. It was shown that the nonlinear portions of the stress and strain curves are sensitive to the strain rate. When the strain rate increases, the material become stiffer. At strain rages less than 1%, it can be shown that the model predictions demonstrate good agreements with experimental results. However, at higher strain level, the predictions deviate from the experiments. This disparity can be attributed to the formation of micro-cracking in the laminates, such as delamination and matrix cracking, which may lead to the stiffness degradation of the whole laminates. Nevertheless, in the model, the laminates were assumed to be damage free and the potential failure mechanisms during the loading process were not considered in analysis.

The stress and strain curves for $[\pm 45]_{3s}$, $[60/-30]_{3s}$, $[\pm 60]_{3s}$ and $[\pm 30]_{3s}$ graphite/epoxy composites obtained from experiments were compared the model prediction in Figure 4.10-4.13, respectively. For $[\pm 45]_{3s}$ and $[60/-30]_{3s}$ laminates, it was indicated that the viscoplasticity model provides fairly good prediction for the rate dependent nonlinearity of the laminate at strain up to 1.2%. Beyond this strain value, the experimental results trend to

soften than the predictions which are similar to those of the glass/epoxy composites. For $[\pm 60]_{3s}$ laminate, specimen failure was happened early because of its $[\pm 60]_{3s}$ stacking sequence characteristic. It is noted that, for $[\pm 30]_{3s}$ laminate, the prediction result is mush softer than experimental results. Therefore, it is possible that other mechanisms are responsible for the discrepancies. In next section, a possible mechanism will be investigated: the deformation-induced fiber orientation change.

4.3 Effect of Deformation-Induced Change of Fiber Orientation

When the laminate specimen is subjected to a tensile loading, the specimen extends in loading direction and contracts in the transverse direction. As a result of this deformation, the fiber orientation will be altered. The detailed description of this effect can be found in Reference [18].

Consider $[\pm\theta]_{ns}$ composite laminates. Figure 4.14a is supposed that the initial fiber orientation in a certain ply is θ. When the laminate is subjected to a tensile loading in the x-direction, the fiber orientation change to θ' (Figure 4.14b). It is easy to derive the relation between θ' and the initial angle θ as:

$$\tan\theta' = \frac{b'}{a'} = \frac{b(1+\varepsilon_y)}{a(1+\varepsilon_x)} = \frac{(1+\varepsilon_y)}{(1+\varepsilon_x)}\tan\theta \qquad (4.1)$$

In an incremental laminate analysis, Equation (4.1) can be used to update the angle of the fiber orientation step-by-step by using the strains from the previous step. Once the new angle is obtained, it is substituted back into the transformation matrix $[T_\sigma]$ and $[T_\varepsilon]$ for updating $[\overline{Q}^{ep}]$ and other quantities. Using such an approach, the effect of fiber orientation change can be included in the laminate model.

Figure 4.15 shows the calculated stress-strain curves with and without the fiber orientation change for $[\pm 30]_{3s}$ graphite/epoxy laminate at strain rate of 0.0001/s. The effect of fiber orientation change is obviously become stiffer in the nonlinear behavior. However, it is still

deviated from the experiments.

4.4 Sensitivity in Stacking Sequence for Symmetric Laminate

In order to understand the sensitivity of the nonlinear behavior to the fiber orientation, $[\pm\theta]_s$ graphite/epoxy laminates with fiber orientations 29°, 30°, 44°, 45°, 59°, and 60° were modeled and shown in Figure 4.16. It is indicated that for $[\pm 29]_s$ and $[\pm 30]_s$ laminates, the nonlinear portions are quite different. However, $[\pm 44]_s$ and $[\pm 45]_s$ illustrate almost the same stress and strain curves which is similar to those in $[\pm 59]_s$ and $[\pm 60]_s$ laminates. As a result, among the angle-ply laminates considered, the stress and strain curve of $[\pm 30]_s$ demonstrate the strong dependence on the fiber orientation.

Prior to the tests conducted, we took the $[\pm 30]_{3s}$ specimen and observed the corresponding fiber angles in each ply with respect to the loading direction using the optical microscope. The measured angles of each ply were shown in Figure 4.17. The calculation of average value of each angle is 29.08° for nominal $[\pm 30]_s$ laminates. Based on this measurement, the new model prediction with initial fiber orientation of 29° was performed. The deformation induced fiber orientation change was also considered in the prediction as shown in Figure 4.18. It was shown the predictions are getting close to the experimental results, however, still have discrepancy existing at the high strain level.

V. Conclusion

A constitutive model was proposed based on the viscoplasticity model and the laminated plate theory for characterizing the nonlinear rate dependent behavior of composite laminates. In the viscoplasticity model, the correlation between effective stress and effective plastic strain was established in the form of power law with rate dependent amplitude and the associated parameters were determined by testing the off-axis coupon specimens at strain rates of 0.0001/s, 0.001/s, and 1/s. With a numerical iteration on the incremental form of the constitutive model, the stress-strain relations of the composite laminates at various strain rates can be generated. In order to demonstrate the strain rate effect, glass/epoxy composite laminates ($[\pm 45/90_2]_{4s}$, $[75_2/-60/30]_{4s}$, and $[60_2/-75/15]_{4s}$) and graphite/epoxy composite laminates ($[\pm 45]_{3s}$, $[60/-30]_{3s}$, $[\pm 60]_{3s}$ and $[\pm 30]_{3s}$) were tested at three different strain rates. Experimental results reveal that the nonlinear portions of the stress-strain curves are pretty sensitive to the strain rates. Comparison of model predictions with experiments indicates that the constitutive model is capable of predicting the nonlinear rate dependent behavior pf composite laminates at strain rates up to 1/s. It is noted that, for $[\pm 30]_{3s}$ graphite/epoxy laminate, the nonlinearity is quite sensitive to the fiber orientation, therefore, a precise measurement of the off-axis angle as well as accounting the effect of deformation induced fiber orientation change are required for model the stress and strain relation.

Reference

[1] Wu, J. F., Shephard, M. S., Dvorak, G. J., and Bahei-Ei-Din, Y. A. 1989 "A material Model for the Finite Element Analysis of Metal Matrix Composites," *Composites Science and Technology*, Vol. 35, pp. 347-366.

[2] Sun, C. T. and Vaidya R. S. 1996 "Prediction of Composite Properties from a Representative Volume Element," *Composites Science and Technology*, Vol. 56, pp. 171-179.

[3] Zhu, C. and Sun, C. T. 2003 "Micromechanical Modeling of Fiber Composites Under Off-Axis Loading," *Journal of Thermoplastic Composite Materials*, Vol. 16, pp. 333-344.

[4] Aboudi, J. 1987 "Closed Form Constitutive Equations for Metal Matrix Composites," *International journal of engineering science*, Vol. 25, No. 9, pp. 1229-1240.

[5] Sun, C. T. and Chen, J. L. 1991 "A Micromechanical Model for Plastic Behavior of Fibrous Cimposites," *Composites Science and Technology*, Vol. 40, pp. 115-129.

[6] Hahn, H. T. and Tsai, S. W. 1973 "Nonlinear Elastic Behavior of Unidirectional Composite laminae," *Journal of Composites Materials*, Vol. 7, pp. 102-118.

[7] Lin, W. P. and Hu, H. T. 2002 "Nonlinear Analysis of Fiber-Reinforced Composite Laminates Subjected to Uniaxial Tensile Load," *Journal of Composite Materials*, Vol. 36, pp. 1429-1450.

[8] Vaziri, R., Olson, M. D., and Anderson, D. L. 1991 "A Plasticity-Based Constitutive Model for Fibre-Reinforced Composite Laminates," *Journal of Composites Materials*, Vol. 25, pp. 512-535.

[9] Hansen, A. C., Blackketter, D. M., and Walrath, D. E. 1991 "An Invariant-Based Flow Rule for Anisotropic Plasticity Applied to Composite Materials," *Journal of Applied Mechanics*, Vol. 58, pp. 881-888.

[10] Sun, C. T. and Chen, J. L. 1989 "A Simple Flow Rule for Characterizing Nonlinear Behavior of Fiber Composites," *Journal of Composites Materials*, Vol. 23, pp.1009-1020.

[11] Ogi, K. and Takeda, N. 1997 "Effects of Moisture Content on Nonlinear Deformation Behavior of CF/Epoxy Composites," *Journal of Composite Materials*, Vol. 31, No. 6, pp. 530-551.

[12] Sun, W. and Lau, A. C. W. 2002 "Three-Dimensional Constitutive Model for Anisotropic Inelastic Deformation of Unidirectional Reinforced Composites," *Journal of Thermoplastic Composite Materials*, Vol. 15, pp. 477-496.

[13] Ogihara, S., Kobayashi, S., and Reifsnider, K. L. 2003 "Characterization of Nonlinear Behavior of Carbon/Epoxy Unidirectional and Angle-Ply Laminates" *Advanced Composite Materials*, Vol. 11, No. 3, pp. 239-254.

[14] Bodner, S. R. and Partom, Y. 1975 "Constitutive Equations for Elastic-Viscoplastic Strain-Hardening Materials," *Journal of Applied Mechanics*, June, 385-389.

[15] Yoon, K. J. and Sun, C. T. 1991 "Characterization of Elastic-Viscoplastic Properties of an AS4/PEEK Thermoplastic Composite," *Journal of Composite Materials*, Vol. 25. pp. 1277-1296.

[16] Gates, T. S. and Sun, C. T. 1991 "Elastic/Viscoplastic Constitutive Model for Fiber Reinforced Thermoplastic Composites," *AIAA Journal*, Vol. 29, No. 3, pp. 457-463.

[17] Zhu, C. and Sun, C. T. 2000 "Viscoplasticity Model for Characterizing Loading and Unloading Behavior of Polymeric Composites," *ASTM Special Technical Publication*, No. 1357, pp. 266-284.

[18] Sun, C. T. and Zhu, C. 2000 "The Effect of Deformation-Induced Change of Fiber Orientation on the Non-Linear Behavior of Polymeric Composite Laminates," *Composites Science and Technology*, Vol. 60, pp. 2337-2345.

[19] Thiruppukuzhi, S. V. and Sun, C. T. 2001 "Models for the Strain-Rate-Dependent Behavior of Polymer composites," *Composites Science and Technology*, Vol. 61, pp. 1-12.

[20] Tsai, J. L. and Sun, C. T. 2002 "Constitutive Model for High Strain Rate Response of Polymeric Composites," *Composites Science and Technology*, Vol. 62, pp. 1289-1297.

[21] Hill, R., The Mathematical Theory of Plasticity, Oxford University Press., London, 1950.

[22] Khan, A. S. and Huang, S., Continuum Theory of Plasticity, A Wiley-Interscience Publication, Canada, 1995.

[23] Gibson, R. F. 1994, *Principles of Composite Material Mechanics*, McGraw-Hill, Inc., New York.

[24] Sun, C. T. and Chung I. 1993 "An Oblique End-Tab Design for Testing Off-axis Composite Specimens," *Composite*, Vol. 24, No. 8, pp. 619-623.

[25] Scalea, F. L. D. 1998 "Measurement of Thermal Expansion Coefficients of Composites Using Strain Gages," *Experimental Mechanics*, Vol. 38, No. 4, pp. 233-241.

[26] 1987 "Measurement of Thermal Expansion Coefficient Using Strain Gages", Micro-Measurement Technical Note TN-513, Measurement Group, Inc.

[27] Tuttle, M. E. 1989 "Fundamental Strain-Gage Technology," *Manual on Experiment Methods for Mechanical Testing of Composites*, edited by Pendleton, R. L. and Tuttle, M. E., Society for Experimental Mechanics, Bethel, CT.

Appendix

A. Thermal Residual Stresses in Composite Laminates

From equations (2.20), (2.27), and (2.28), it is known that the laminate stiffness matrix [*R*] is related with the current stress state in each ply of laminate. Therefore, now we consider the corresponding thermal residual stresses in laminates due to interaction with other laminae. Because of differences between fiber and matrix CTEs (coefficients of thermal expansion) in the lamina and differences between lamina CTEs in the laminate, residual stresses may occur during fabrication with temperature change. The total strains in the *k*th ply are given the form when changes in temperature occur:

$$\begin{Bmatrix} \varepsilon_{xx} \\ \varepsilon_{yy} \\ \gamma_{xy} \end{Bmatrix}_k = \left[\bar{S}\right]_k \begin{Bmatrix} \sigma_{xx} \\ \sigma_{yy} \\ \sigma_{xy} \end{Bmatrix}_k + \begin{Bmatrix} \alpha_{xx} \\ \alpha_{yy} \\ \alpha_{xy} \end{Bmatrix}_k \Delta T \tag{A.1}$$

and the resulting stresses are given by

$$\begin{Bmatrix} \sigma_{xx} \\ \sigma_{yy} \\ \sigma_{xy} \end{Bmatrix}_k = \left[\bar{Q}\right]_k \left(\begin{Bmatrix} \varepsilon_{xx} \\ \varepsilon_{yy} \\ \gamma_{xy} \end{Bmatrix}_k - \begin{Bmatrix} \alpha_{xx} \\ \alpha_{yy} \\ \alpha_{xy} \end{Bmatrix}_k \Delta T \right)$$

$$= \left[\bar{Q}\right]_k \left(\begin{Bmatrix} \varepsilon^0_{xx} \\ \varepsilon^0_{yy} \\ \gamma^0_{xy} \end{Bmatrix} + z\{\kappa\} - \begin{Bmatrix} \alpha_{xx} \\ \alpha_{yy} \\ \alpha_{xy} \end{Bmatrix}_k \Delta T \right) \tag{A.2}$$

In the transformations it must be noted that the CTEs transform like tensor strains, so that

$$\begin{Bmatrix} \alpha_x \\ \alpha_y \\ \alpha_{xy} \end{Bmatrix} = \begin{Bmatrix} \alpha_1 \cos^2\theta + \alpha_2 \sin^2\theta \\ \alpha_1 \sin^2\theta + \alpha_2 \cos^2\theta \\ 2(\alpha_1 - \alpha_2)\cos\theta \sin\theta \end{Bmatrix} \tag{A.3}$$

The resultant laminate forces $\{N\}$ and moment $\{M\}$ per unit length are found by integrating equation (A.2) though the thickness of laminate and rearranged:

$$\begin{Bmatrix} N \\ M \end{Bmatrix} = \begin{bmatrix} A & B \\ B & D \end{bmatrix} \begin{Bmatrix} \varepsilon^0 \\ \kappa \end{Bmatrix} - \begin{Bmatrix} N^T \\ M^T \end{Bmatrix} \tag{A.4}$$

where the thermal forces: $\{N^T\} = \int [\overline{Q}]_k \{\alpha\}_k \Delta T dz$ (A.5)

and the thermal moments: $\{M^T\} = \int [\overline{Q}]_k \{\alpha\}_k \Delta T z dz$ (A.6)

Alternatively, the inverted forms of equation (A.4) are given by

$$\begin{Bmatrix} \varepsilon^0 \\ \kappa \end{Bmatrix} = \begin{bmatrix} A & B \\ B & D \end{bmatrix}^{-1} \left(\begin{Bmatrix} N \\ M \end{Bmatrix} + \begin{Bmatrix} N^T \\ M^T \end{Bmatrix} \right) \tag{A.7}$$

Let the mechanical loading be zero for the initial thermal residual stress state, i.e. $\{N\} = \{0\}$, $\{M\} = \{0\}$, and considering symmetric laminate for simplicity, i.e. $\{M^T\} = \{0\}$, $\{B\} = \{0\}$. Substitution into equation (A.7) with above assumptions, we can get the following relations.

$$\{\varepsilon^0\} = [A]^{-1} \{N^T\} \tag{A.8}$$

$$\{\kappa\} = \{0\} \tag{A.9}$$

It means that no out of plane deformation occurs in symmetric laminate when have uniform temperature change. The strain in mid-plane represents the laminate strain in each ply. Finally, substitution the thermal-induced deformation in laminate into equation (A.2), the laminar residual stress in each ply is

$$\{\sigma^r\}_k = [\overline{Q}]_k \begin{Bmatrix} \varepsilon_x^0 - \alpha_x \Delta T \\ \varepsilon_y^0 - \alpha_y \Delta T \\ \gamma_{xy}^0 - \alpha_{xy} \Delta T \end{Bmatrix} \tag{A.10}$$

The calculated $\{\sigma^r\}_k$ will be the initial stress state in *k*th ply of laminate. They are inputted to the numerical process as the initial stress variables before the loading increment was applied.

B. Numerical Code

```
%simple flow rule for characterizing nonlinear behavior of graphite/epoxy laminates
%-------------------------------------------------------------------------
% symbols:
% e1,e2,g12,v12,v21,a66,n,x: material parameters
% ta1,ta2: thermal expansion coefficients in fiber and transverse direction
% tdt: temperature change
% exp: stress-strain form experiment
% datanum: numbers of exp. data
% ang1~ang4:ply 1~4 angle
% rad1~rad4:ply 1~4 radian
% delta1,delta2: the incremental stress
% final1,final2: the final stress
% q00: 0 degree Q stiffness matrix
% qc1~qc4: ang1~ang4 Q-bar stiffness matrix
% tsig1~tsig4: ang1~ang4 stress components coordinate transformation matrix
% teps1~teps4: ang1~ang4 strain components coordinate transformation matrix
% sig1~sig4: ang1~ang4 stress components in x1-x2 coordinate
% eps1~eps4: ang1~ang4 strain components in x1-x2 coordinate
% sigxy: laminate average stress cpmponents
% epsxy: laminate strain components
% dsigxy: the incremental laminate average stress components in x-y coordinate
% depsxy: the incremental strain components in x-y coordinate
% effsig1~effsig4: effective stress in ang1~ang4
% sep1~sep4: elastic-plastic compliance matrix in ang1~ang4
% qep1~qep4: elastic-plastic stiffness matrix in ang1~ang4
% g: laminate stiffness matrix
% dsigtxy1~dsigtxy4: the incremental stress components in ang1~ang4 on x-y coordinate
% dsig1~dsig4: the incremental stress components in ang1~ang4 on 1-2 coordinate
%-------------------------------------------------------------------------
clear all;
%---------------------------------------- material properties--------------------
e1=138.5e3;
e2=8.1e3;
g12=4.2e3;
v12=0.27;
```

```
v21=v12*e2/e1;
a66=1.6;
n=4.6;
x=0.7e-12;
m=-0.185;
ta1=0.57e-6;                    %thermal expansion coefficient
ta2=41.4e-6;                    %thermal expansion coefficient
tdt=-125;                       %temperature change
%---------------------------------------- material properties--------------------
%------------------input stress rate data from experimental results---------
fid=fopen('pn60_high.txt');
datanum=57;
exp=fscanf(fid,'%g',[2 datanum]);
exp=exp';
redu=1;
nn=(datanum-1)/redu;
dt=(exp(2,1)-exp(1,1))*redu;
rate=1e-20;
%------------------input stress rate data from experimental results---------
%-----------------------stacking sequences--------------
ang1=60;
ang2=-60;
ang3=-60;
ang4=60;
%-----------------------stacking sequences---------------
i=[1 0 0;0 1 0;0 0 1];      %unit matrix
q11=e1/(1-v12*v21);
q12=v12*e2/(1-v12*v21);
q21=q12;
q22=e2/(1-v12*v21);
q33=g12;
q00=[q11 q12 0;q21 q22 0; 0 0 q33];                    %0 degree stiffness matrix
u1=(3*q11+3*q22+2*q12+4*q33)/8;
u2=(q11-q22)/2;
u3=(q11+q22-2*q12-4*q33)/8;
u4=(q11+q22+6*q12-4*q33)/8;
rad1=ang1*pi/180;
rad2=ang2*pi/180;
```

```
rad3=ang3*pi/180;
rad4=ang4*pi/180;
q1=u1+u2*cos(2*rad1)+u3*cos(4*rad1);
q2=u4-u3*cos(4*rad1);
q3=u1-u2*cos(2*rad1)+u3*cos(4*rad1);
q4=sin(2*rad1)*u2/2+u3*sin(4*rad1);
q5=sin(2*rad1)*u2/2-u3*sin(4*rad1);
q6=(u1-u4)/2-u3*cos(4*rad1);
qc1=[q1 q2 q4;
     q2 q3 q5;
     q4 q5 q6;];                          %1-th ply off-axis stiffness matrix
q1=u1+u2*cos(2*rad2)+u3*cos(4*rad2);
q2=u4-u3*cos(4*rad2);
q3=u1-u2*cos(2*rad2)+u3*cos(4*rad2);
q4=sin(2*rad2)*u2/2+u3*sin(4*rad2);
q5=sin(2*rad2)*u2/2-u3*sin(4*rad2);
q6=(u1-u4)/2-u3*cos(4*rad2);
qc2=[q1 q2 q4;
      q2 q3 q5;
      q4 q5 q6;];                         %2-th ply off-axis stiffness matrix
q1=u1+u2*cos(2*rad3)+u3*cos(4*rad3);
q2=u4-u3*cos(4*rad3);
q3=u1-u2*cos(2*rad3)+u3*cos(4*rad3);
q4=sin(2*rad3)*u2/2+u3*sin(4*rad3);
q5=sin(2*rad3)*u2/2-u3*sin(4*rad3);
q6=(u1-u4)/2-u3*cos(4*rad3);
qc3=[q1 q2 q4;
     q2 q3 q5;
     q4 q5 q6;];                          %3-th ply off-axis stiffness matrix
q1=u1+u2*cos(2*rad4)+u3*cos(4*rad4);
q2=u4-u3*cos(4*rad4);
q3=u1-u2*cos(2*rad4)+u3*cos(4*rad4);
q4=sin(2*rad4)*u2/2+u3*sin(4*rad4);
q5=sin(2*rad4)*u2/2-u3*sin(4*rad4);
q6=(u1-u4)/2-u3*cos(4*rad4);
qc4=[q1 q2 q4;
      q2 q3 q5;
      q4 q5 q6;];                         %4-th ply off-axis stiffness matrix
```

```
%1-th ply CTE coordinate transformation
 ac1=[ta1*cos(rad1)^2+ta2*sin(rad1)^2;
      ta1*sin(rad1)^2+ta2*cos(rad1)^2;
      2*(ta1-ta2)*cos(rad1)*sin(rad1)];
%2-th ply CTE coordinate transformation
ac2=[ta1*cos(rad2)^2+ta2*sin(rad2)^2;
       ta1*sin(rad2)^2+ta2*cos(rad2)^2;
       2*(ta1-ta2)*cos(rad2)*sin(rad2)];
%3-th ply CTE coordinate transformation
ac3=[ta1*cos(rad3)^2+ta2*sin(rad3)^2;
      ta1*sin(rad3)^2+ta2*cos(rad3)^2;
      2*(ta1-ta2)*cos(rad3)*sin(rad3)];
%4-th ply CTE coordinate transformation
ac4=[ta1*cos(rad4)^2+ta2*sin(rad4)^2;
       ta1*sin(rad4)^2+ta2*cos(rad4)^2;
       2*(ta1-ta2)*cos(rad4)*sin(rad4)];
%1-th ply coordinate transformation
tsig1=[cos(rad1)^2     sin(rad1)^2     2*sin(rad1)*cos(rad1);
         sin(rad1)^2     cos(rad1)^2    -2*sin(rad1)*cos(rad1);
         -sin(rad1)*cos(rad1)     sin(rad1)*cos(rad1)    (cos(rad1)^2-sin(rad1)^2)];
teps1=[cos(rad1)^2     sin(rad1)^2     sin(rad1)*cos(rad1);
         sin(rad1)^2     cos(rad1)^2    -sin(rad1)*cos(rad1);
         -2*sin(rad1)*cos(rad1)     2*sin(rad1)*cos(rad1)    (cos(rad1)^2-sin(rad1)^2)];
%---------------------------------
%2-th ply coordinate transformation
tsig2=[cos(rad2)^2     sin(rad2)^2     2*sin(rad2)*cos(rad2);
         sin(rad2)^2     cos(rad2)^2    -2*sin(rad2)*cos(rad2);
         -sin(rad2)*cos(rad2)     sin(rad2)*cos(rad2)    (cos(rad2)^2-sin(rad2)^2)];
teps2=[cos(rad2)^2     sin(rad2)^2     sin(rad2)*cos(rad2);
         sin(rad2)^2     cos(rad2)^2    -sin(rad2)*cos(rad2);
         -2*sin(rad2)*cos(rad2)     2*sin(rad2)*cos(rad2)    (cos(rad2)^2-sin(rad2)^2)];
%---------------------------------
%3-th ply coordinate transformation
tsig3=[cos(rad3)^2     sin(rad3)^2     2*sin(rad3)*cos(rad3);
         sin(rad3)^2     cos(rad3)^2    -2*sin(rad3)*cos(rad3);
         -sin(rad3)*cos(rad3)     sin(rad3)*cos(rad3)    (cos(rad3)^2-sin(rad3)^2)];
teps3=[cos(rad3)^2     sin(rad3)^2     sin(rad3)*cos(rad3);
         sin(rad3)^2     cos(rad3)^2    -sin(rad3)*cos(rad3);
```

```
        -2*sin(rad3)*cos(rad3)     2*sin(rad3)*cos(rad3)    (cos(rad3)^2-sin(rad3)^2)];
%---------------------------------
%4-th ply coordinate transformation
tsig4=[cos(rad4)^2      sin(rad4)^2      2*sin(rad4)*cos(rad4);
        sin(rad4)^2      cos(rad4)^2    -2*sin(rad4)*cos(rad4);
        -sin(rad4)*cos(rad4)      sin(rad4)*cos(rad4)    (cos(rad4)^2-sin(rad4)^2)];
teps4=[cos(rad4)^2      sin(rad4)^2      sin(rad4)*cos(rad4);
        sin(rad4)^2      cos(rad4)^2    -sin(rad4)*cos(rad4);
        -2*sin(rad4)*cos(rad4)      2*sin(rad4)*cos(rad4)    (cos(rad4)^2-sin(rad4)^2)];
%---------------------------------
sig1=[0;0;0];                          %1-th initial stress, strain tensor
eps1=[0;0;0];
sig2=[0;0;0];                          %2-th initial stress, strain tensor
eps2=[0;0;0];
sig3=[0;0;0];                          %3-th initial stress, strain tensor
eps3=[0;0;0];
sig4=[0;0;0];                          %4-th initial stress, strain tensor
eps4=[0;0;0];
%----calculation of thermal residual stress----------
ma=8*qc1+8*qc2+8*qc3+8*qc4;
nt=(qc1*ac1+qc2*ac2+qc3*ac3+qc4*ac4)*8*tdt;
thermaldepsxy=inv(ma)*nt;
resigxy1=qc1*(thermaldepsxy-ac1*tdt);
resigxy2=qc2*(thermaldepsxy-ac2*tdt);
resigxy3=qc3*(thermaldepsxy-ac3*tdt);
resigxy4=qc4*(thermaldepsxy-ac4*tdt);
resig1=tsig1*resigxy1;
resig2=tsig2*resigxy2;
resig3=tsig3*resigxy3;
resig4=tsig4*resigxy4;
%----calculation of thermal residual stress----------
sig1=resig1;
sig2=resig2;
sig3=resig3;
sig4=resig4;
%----calculation of thermal residual stress----------
sigxy(:,1)=[0;0;0];                %set initial zero of laminate stress and strain
epsxy(:,1)=[0;0;0];
```

```
%--------initial value of updated A in each ply---------
      effdepsp1(1)=rate;
      a1=x*effdepsp1(1)^m;
      effdepsp2(1)=rate;
      a2=x*effdepsp2(1)^m;
      effdepsp3(1)=rate;
      a3=x*effdepsp3(1)^m;
      effdepsp4(1)=rate;
      a4=x*effdepsp4(1)^m;
      %pause
%--------initial value of updated A in each ply---------
for k=1:nn;                          %accumulated loops
      dsigxy=[(exp(redu*k+1,2)-exp(redu*(k-1)+1,2)); 0; 0];
%the incremental stress in time interval(x-y coordinate)
      efsig1=(3/2*(sig1(2)^2+2*a66*sig1(3)^2))^0.5;                %ang1 effective stress
      mu1=[0                    0                    0;
          0              9/4*sig1(2)^2     9/2*a66*sig1(2)*sig1(3);
          0     9/2*a66*sig1(2)*sig1(3)     9*a66^2*sig1(3)^2]*a1*n*efsig1^(n-3);
      sep1=teps1^-1*(q00^-1+mu1)*tsig1;                %ang1 elastic-plastic compliance matrix
      qep1=sep1^-1;
      efsig2=(3/2*(sig2(2)^2+2*a66*sig2(3)^2))^0.5;                %ang2 effective stress
      mu2=[0                    0                    0;
          0              9/4*sig2(2)^2     9/2*a66*sig2(2)*sig2(3);
          0     9/2*a66*sig2(2)*sig2(3)     9*a66^2*sig2(3)^2]*a2*n*efsig2^(n-3);
      sep2=teps2^-1*(q00^-1+mu2)*tsig2;                %ang2 elastic-plastic compliance matrix
      qep2=sep2^-1;
      efsig3=(3/2*(sig3(2)^2+2*a66*sig3(3)^2))^0.5;                %ang3 effective stress
      mu3=[0                    0                    0;
          0              9/4*sig3(2)^2     9/2*a66*sig3(2)*sig3(3);
          0     9/2*a66*sig3(2)*sig3(3)     9*a66^2*sig3(3)^2]*a3*n*efsig3^(n-3);
      sep3=teps3^-1*(q00^-1+mu3)*tsig3;                %ang3 elastic-plastic compliance matrix
      qep3=sep3^-1;
      efsig4=(3/2*(sig4(2)^2+2*a66*sig4(3)^2))^0.5;                %ang4 effective stress
      mu4=[0                    0                    0;
          0              9/4*sig4(2)^2     9/2*a66*sig4(2)*sig4(3);
          0     9/2*a66*sig4(2)*sig4(3)     9*a66^2*sig4(3)^2]*a4*n*efsig4^(n-3);
      sep4=teps4^-1*(q00^-1+mu4)*tsig4;                %ang4 elastic-plastic compliance matrix
      qep4=sep4^-1;
```

```
%laminate plate theory
r=(qep1+qep2+qep3+qep4)/4;
g=inv(r);
depsxy=g*dsigxy;
dsigtxy1=qep1*depsxy;                    %the increment of stress in ang1 ply
dsigtxy2=qep2*depsxy;                    %the increment of stress in ang2 ply
dsigtxy3=qep3*depsxy;                    %the increment of stress in ang3 ply
dsigtxy4=qep4*depsxy;                    %the increment of stress in ang4 ply
%-----------coordinate transformation from x-y to 1-2 system--------
dsig1=tsig1*dsigtxy1;
dsig2=tsig2*dsigtxy2;
dsig3=tsig3*dsigtxy3;
dsig4=tsig4*dsigtxy4;
%-----------coordinate transformation from x-y to 1-2 system--------
%-----------updated A in each ply--------
depse1=inv(q00)*dsig1;
depse2=inv(q00)*dsig2;
depse3=inv(q00)*dsig3;
depse4=inv(q00)*dsig4;
depsp1=teps1*depsxy-depse1;
depsp2=teps2*depsxy-depse2;
depsp3=teps3*depsxy-depse3;
depsp4=teps4*depsxy-depse4;
%pause
effdepsp1(k+1,1)=(2/3*(depsp1(2)^2+1/2/a66*depsp1(3)^2))^0.5/dt;
a1=x*effdepsp1(k+1,1)^m;
effdepsp2(k+1,1)=(2/3*(depsp2(2)^2+1/2/a66*depsp2(3)^2))^0.5/dt;
a2=x*effdepsp2(k+1,1)^m;
effdepsp3(k+1,1)=(2/3*(depsp3(2)^2+1/2/a66*depsp3(3)^2))^0.5/dt;
a3=x*effdepsp3(k+1,1)^m;
effdepsp4(k+1,1)=(2/3*(depsp4(2)^2+1/2/a66*depsp4(3)^2))^0.5/dt;
a4=x*effdepsp4(k+1,1)^m;
%pause
%-----------updated A in each ply--------
%----------update the stress in each ply--------
sig1=sig1+dsig1;
sig2=sig2+dsig2;
sig3=sig3+dsig3;
```

```
        sig4=sig4+dsig4;
        %----------update the stress in each ply--------
        %stress and strain in laminate areaccumulated
        sigxy(:,k+1)=sigxy(:,k)+dsigxy;
        epsxy(:,k+1)=epsxy(:,k)+depsxy;
end;                            %loop ended
%-----------plot the results-----------
plot(abs(epsxy(1,:)),abs(sigxy(1,:)));
%axis([0,0.016,0,exp(73,2)]);
xlabel('\epsilon_x');
ylabel('\sigma_x(MPa)');
grid on;
epsxy=epsxy';
sigxy=sigxy';
```

Table 1 Material constants for glass/epoxy composites.

E_1(GPa)	55.7±1.1
E_2(GPa)	21.5±0.65
G_{12}(GPa)	6.9
ν_{12}	0.29±0.003
a_{66}	1.4
n	3.9
χ(MPa)$^{-n}$	6.5×10^{-12}
m	-0.125
$\alpha_1(10^{-6}/°C)$	7
$\alpha_2(10^{-6}/°C)$	18.3

Table 2 Material constants for graphite/epoxy composites ($\nu_f = 0.54$).

E_1(GPa)	138.5±7.3
E_2(GPa)	8.1±0.3
G_{12}(GPa)	4.2±0.2
ν_{12}	0.27±0.01
a_{66}	1.6
n	4.6
χ(MPa)$^{-n}$	0.7×10^{-12}
m	-0.185
$\alpha_1(10^{-6}/°C)$	0.57
$\alpha_2(10^{-6}/°C)$	41.4

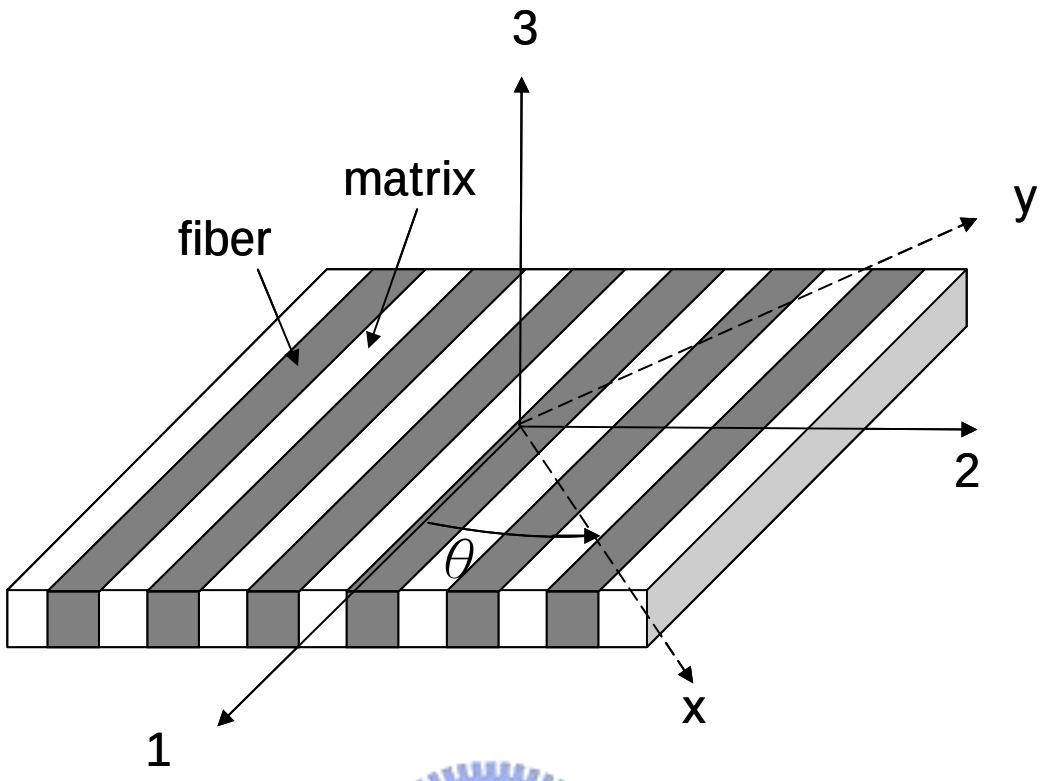

Figure 2.1: Orthotropic lamina with principal and off-axis coordinate systems.

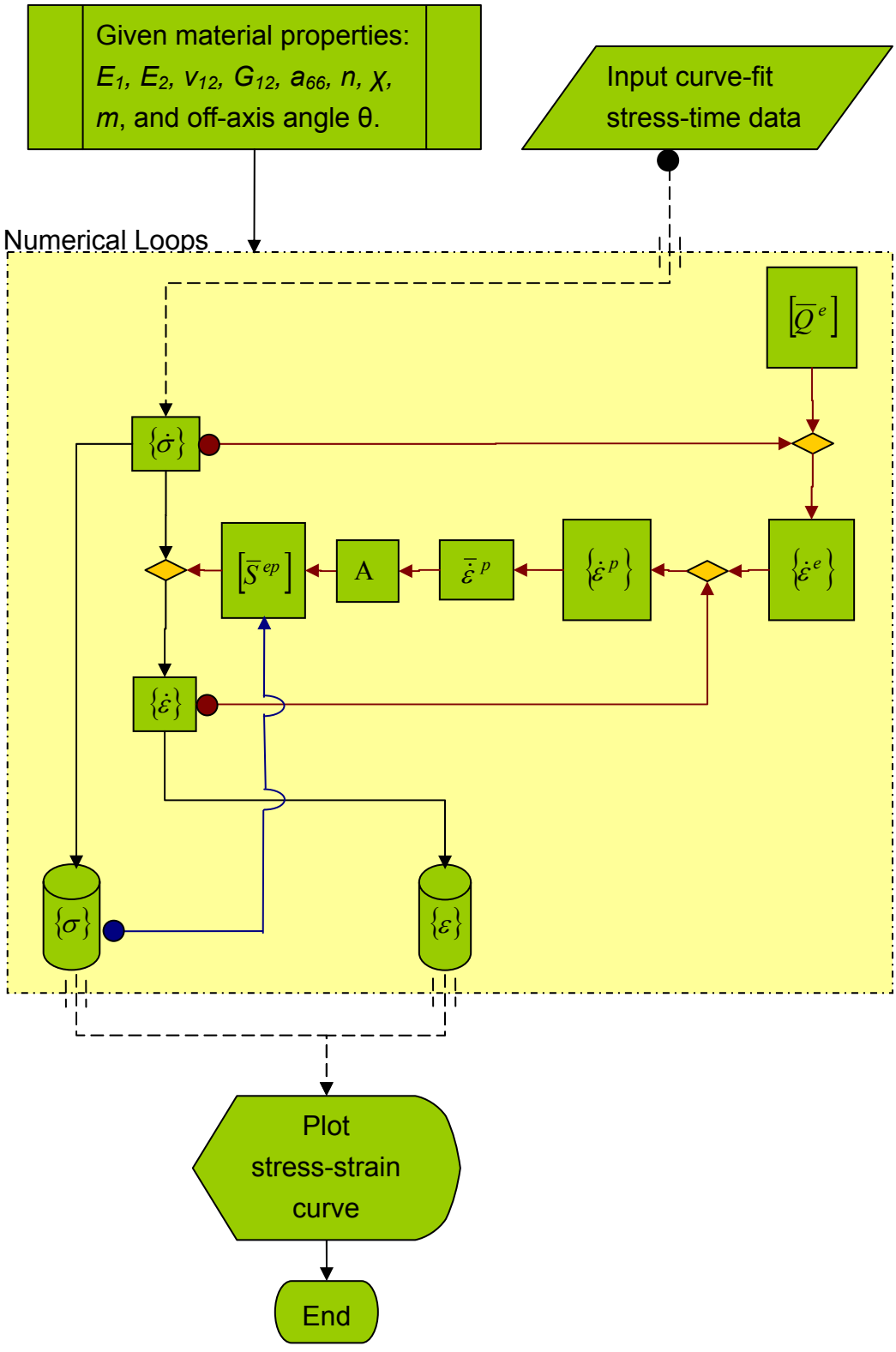

Figure 2.2: Flow chart of the numerical analytic procedure for off-axis composite laminae.

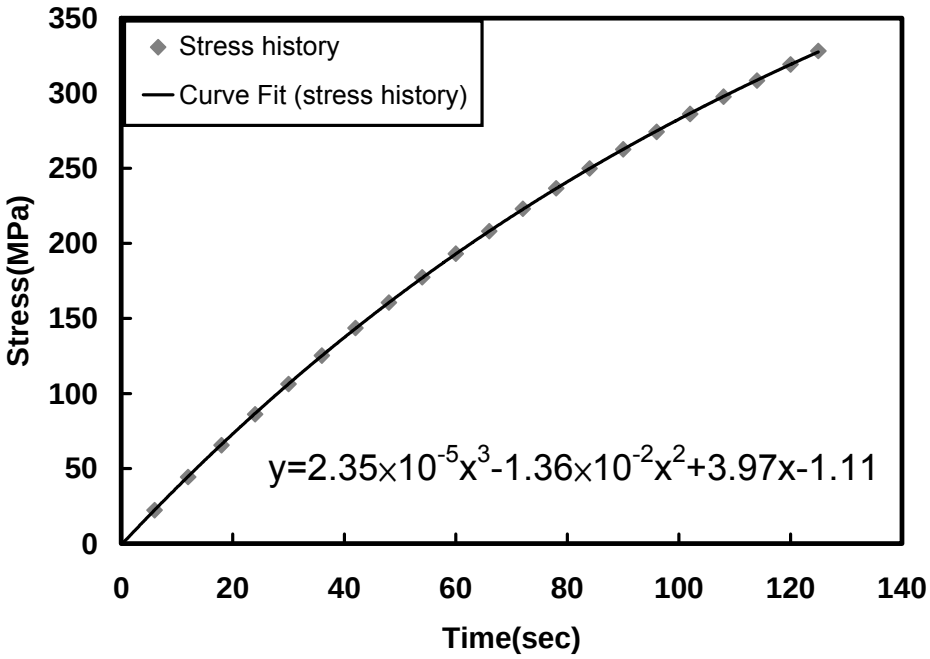

Figure 2.3: example of stress-time for laminate tensile test.

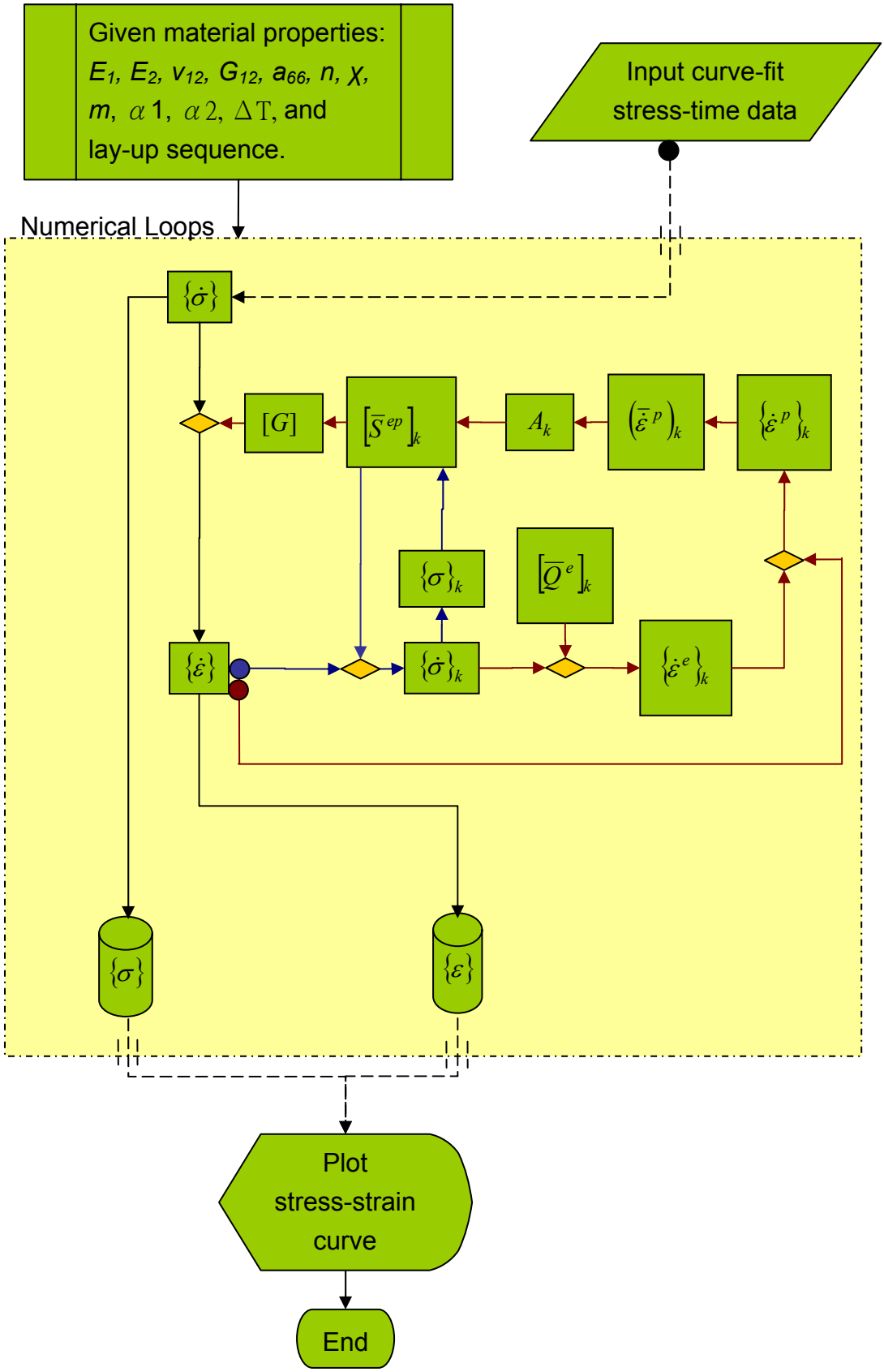

Figure 2.4: Flow chart of the numerical analytic procedure for composite laminates.

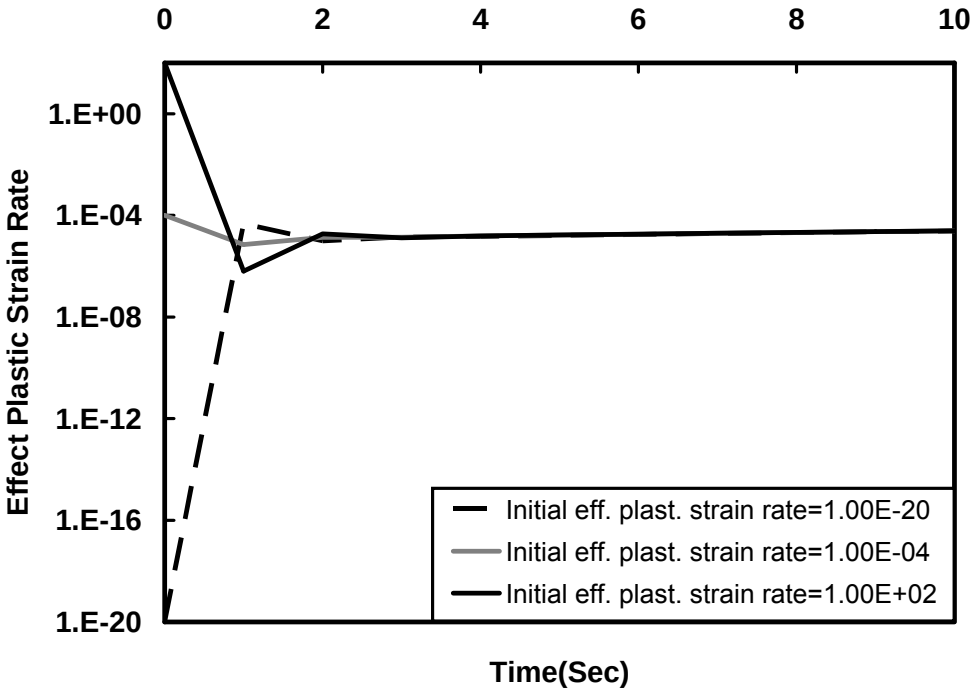

Figure 2.5: the effective plastic strain rate versus time history diagram of $[\pm 30]_{3s}$ graphite/epoxy at strain rate 0.0001/s.

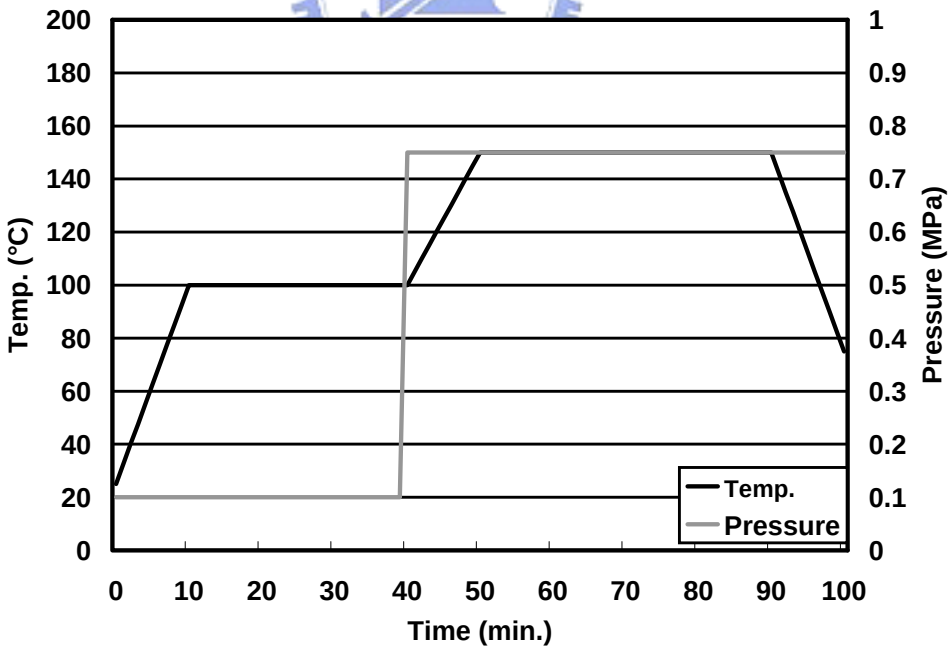

Figure 3.1: Curing process for graphite/epoxy composite prepreg.

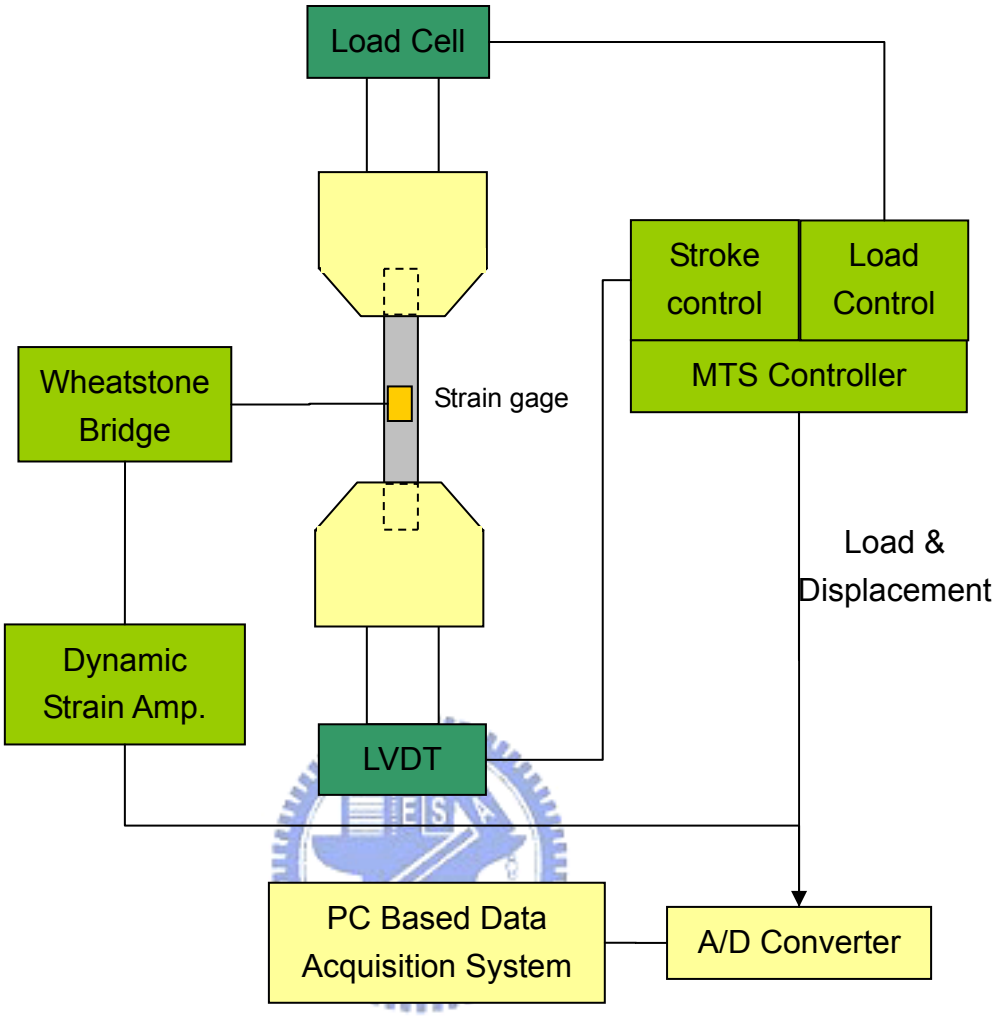

Figure 3.2: Schematic for tension testing system.

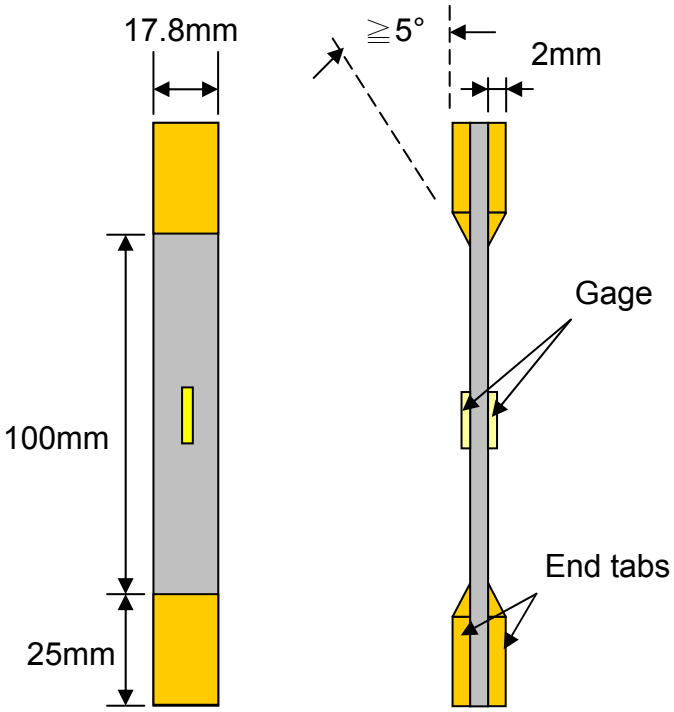

Figure 3.3: Dimensions of tensile test specimen.

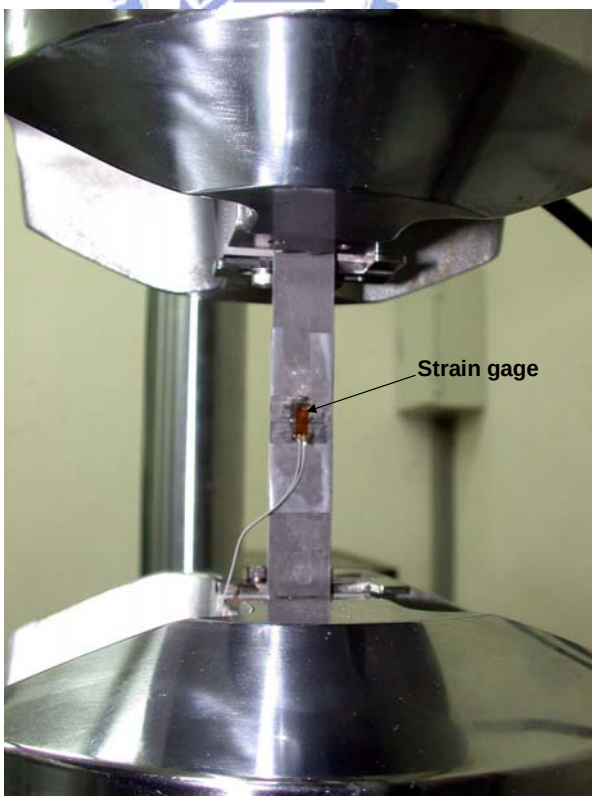

Figure 3.4: Experiment on the MTS 810 machine.

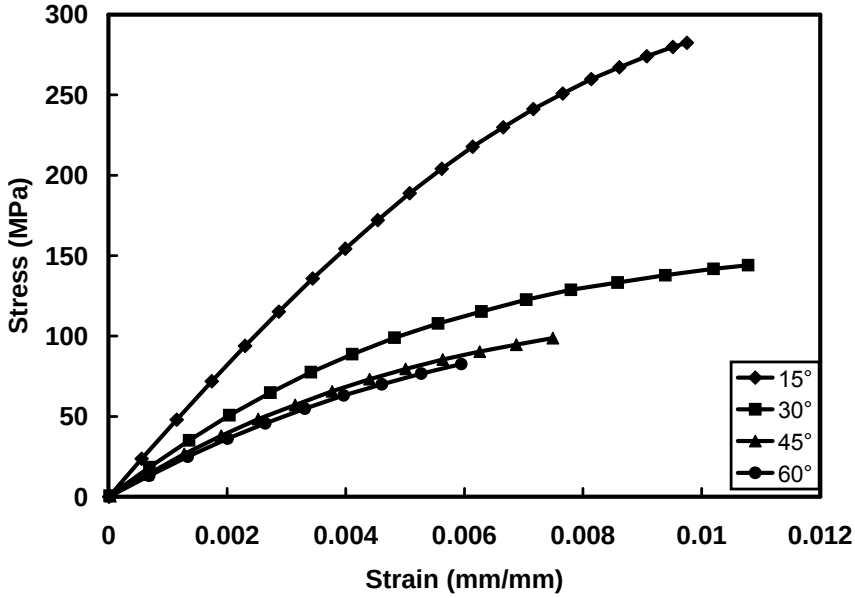

Figure 3.5: Stress-stain curves for glass/epoxy at 0.0001/s.

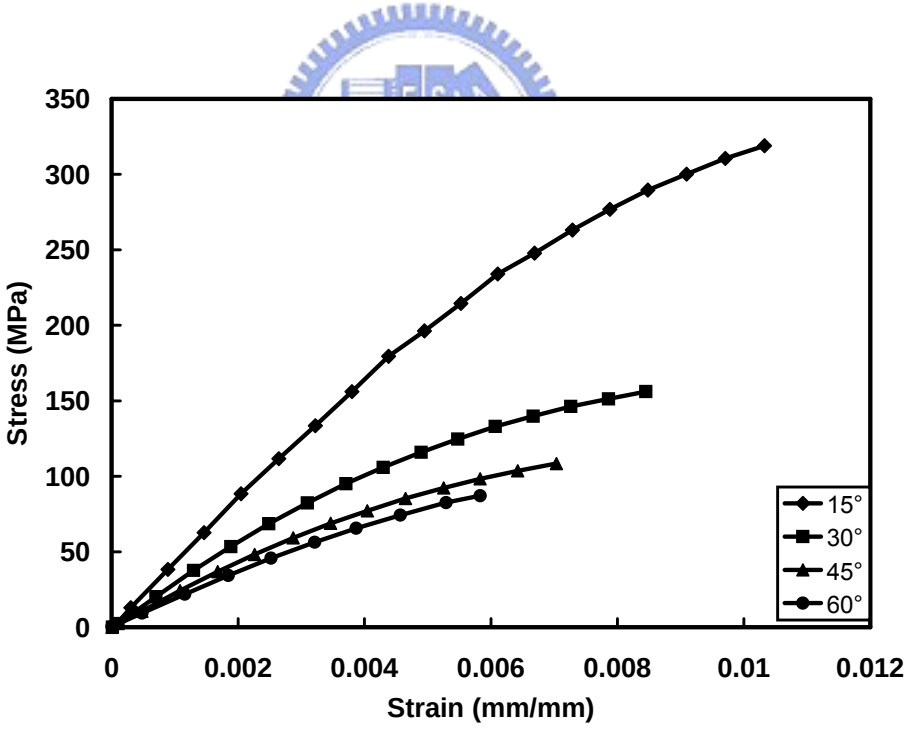

Figure 3.6: Stress-stain curves for glass/epoxy at 0.01/s.

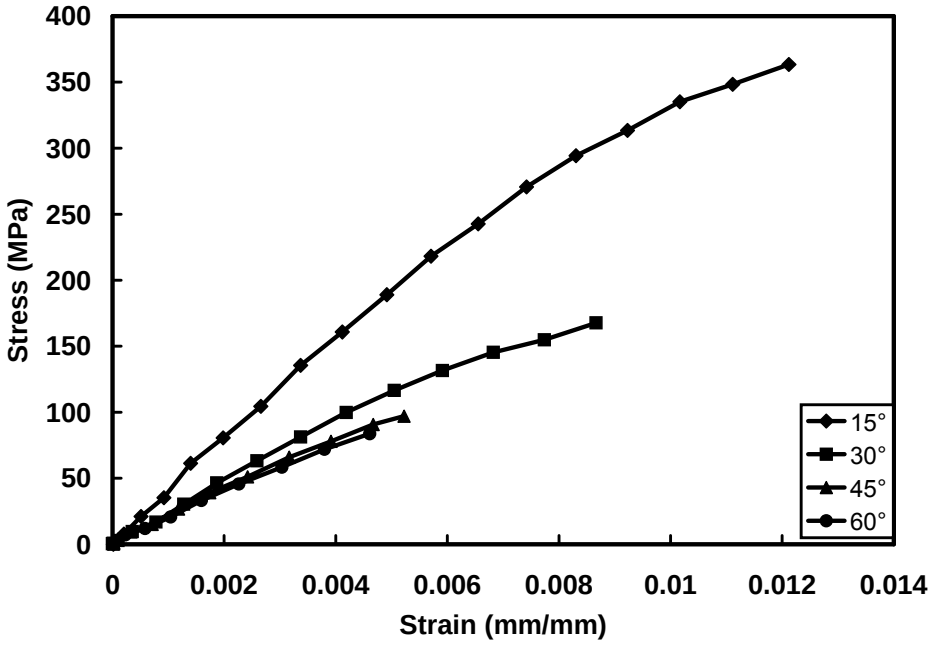

Figure 3.7: Stress-stain curves for glass/epoxy at 1/s.

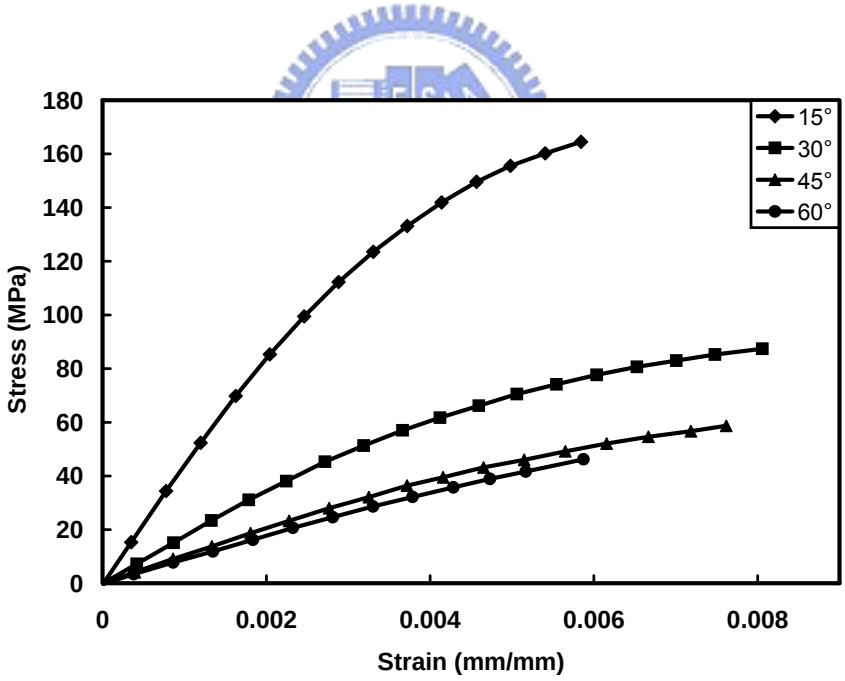

Figure 3.8: Stress-stain curves for graphite/epoxy at 0.0001/s.

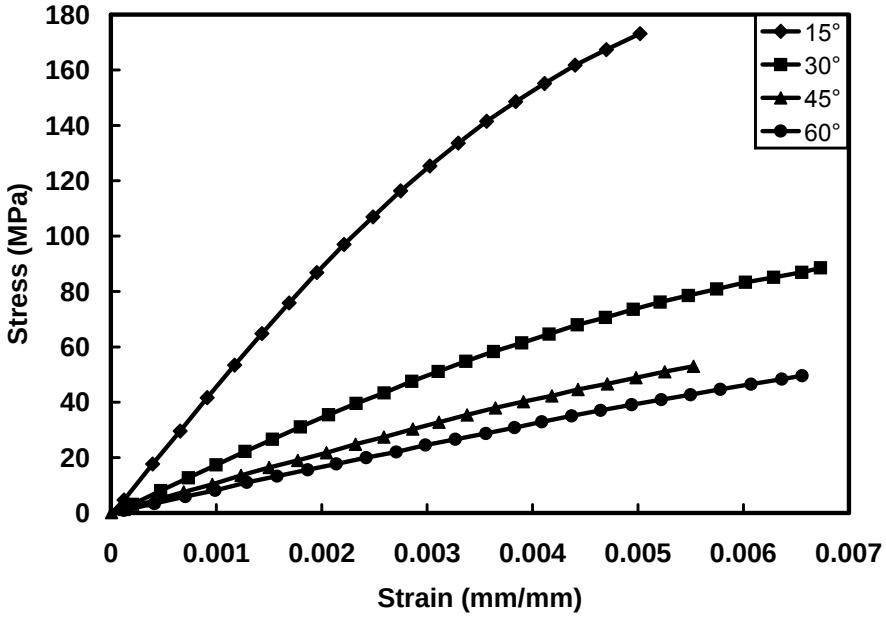

Figure 3.9: Stress-stain curves for graphite/epoxy at 0.01/s.

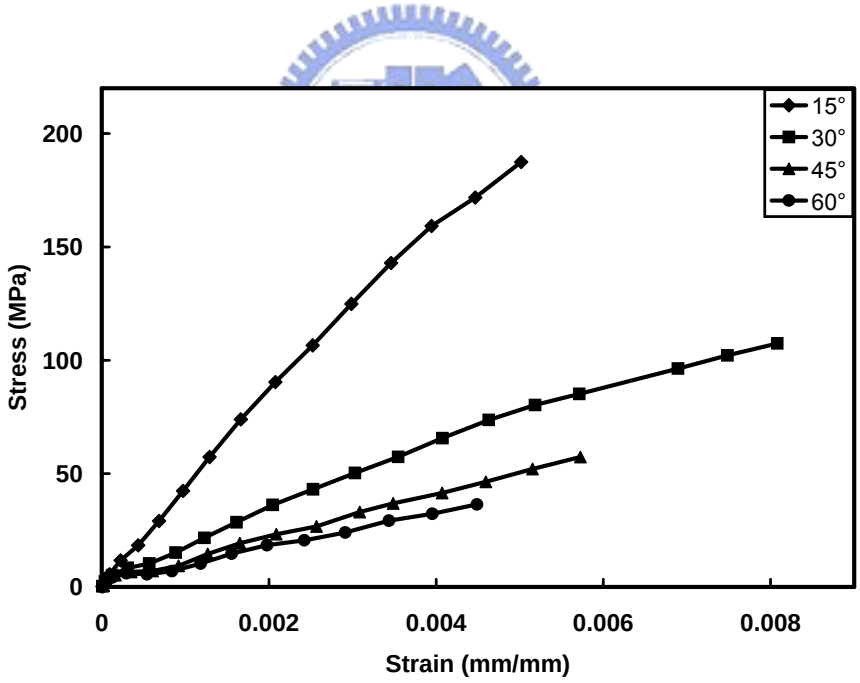

Figure 3.10: Stress-stain curves for graphite/epoxy at 1/s.

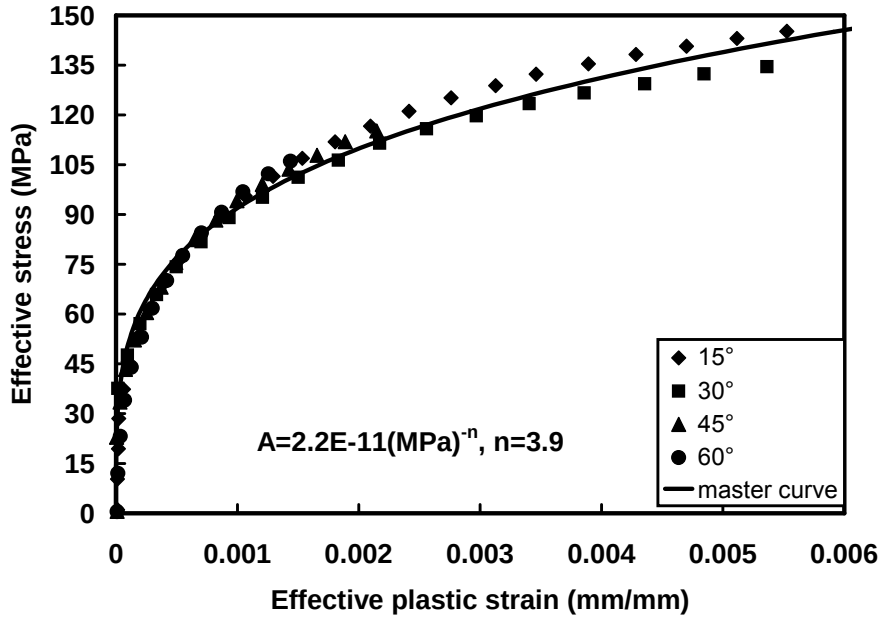

Figure 3.11: Effective stress-effective plastic stain curve for glass/epoxy at 0.0001/s.

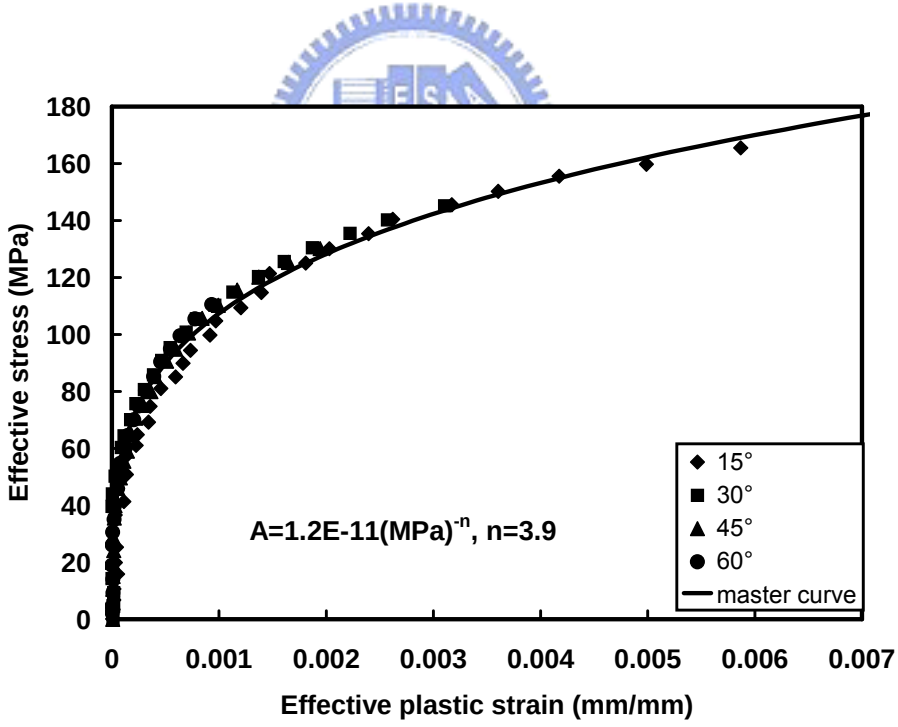

Figure 3.12: Effective stress-effective plastic stain curve for glass/epoxy at 0.01/s.

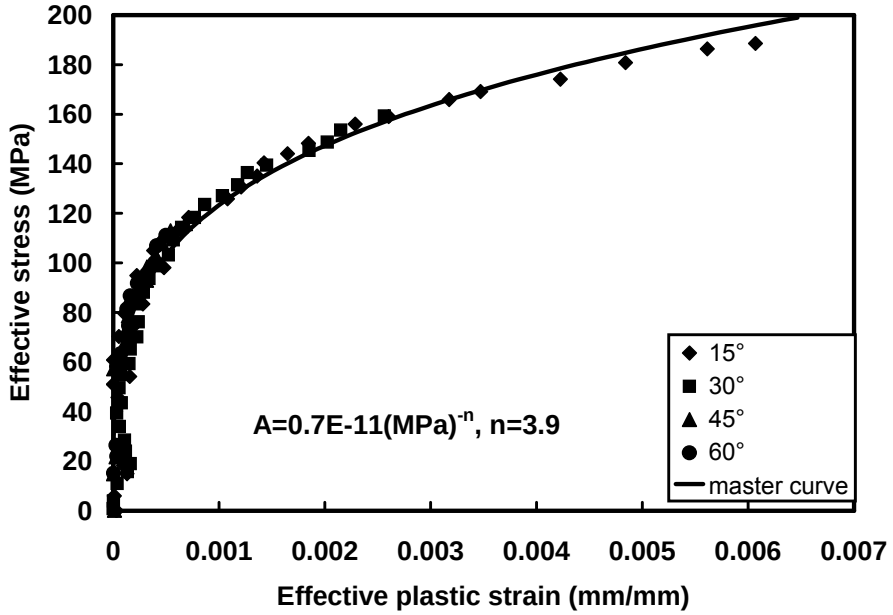

Figure 3.13: Effective stress-effective plastic stain curve for glass/epoxy at 1/s.

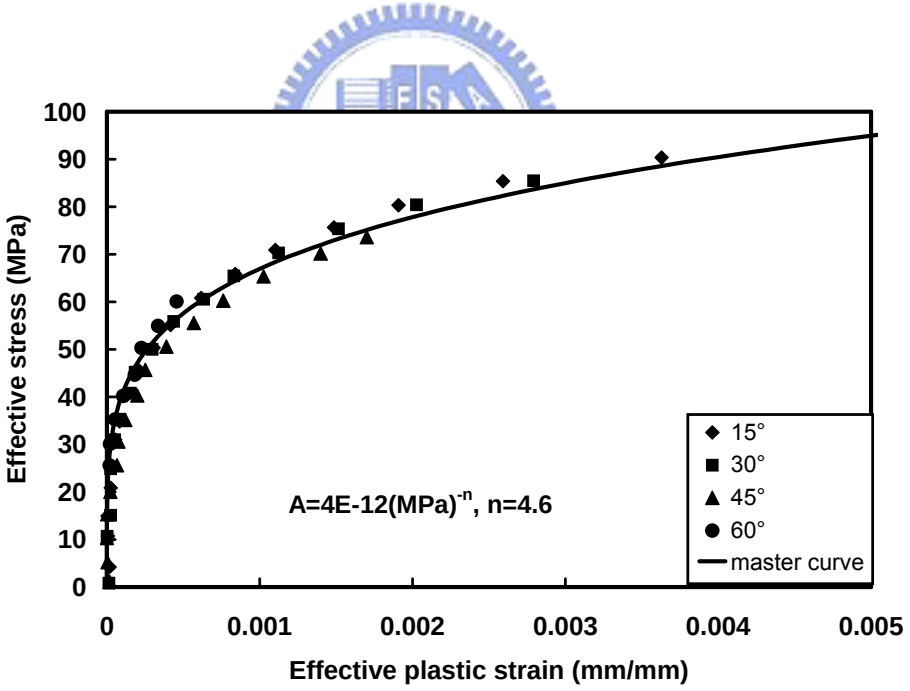

Figure 3.14: Effective stress-effective plastic stain curve for graphite/epoxy at 0.0001/s.

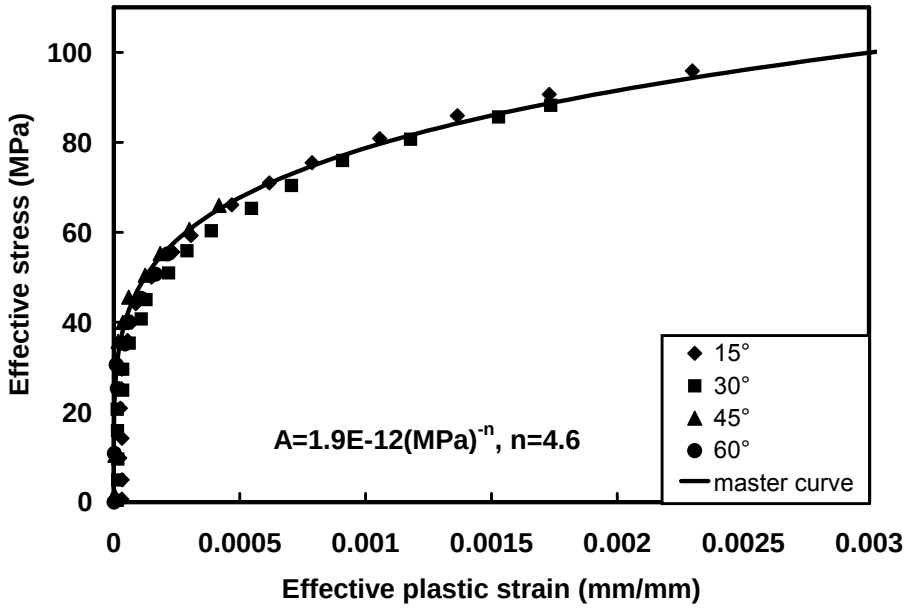

Figure 3.15: Effective stress-effective plastic stain curve for graphite/epoxy at 0.01/s.

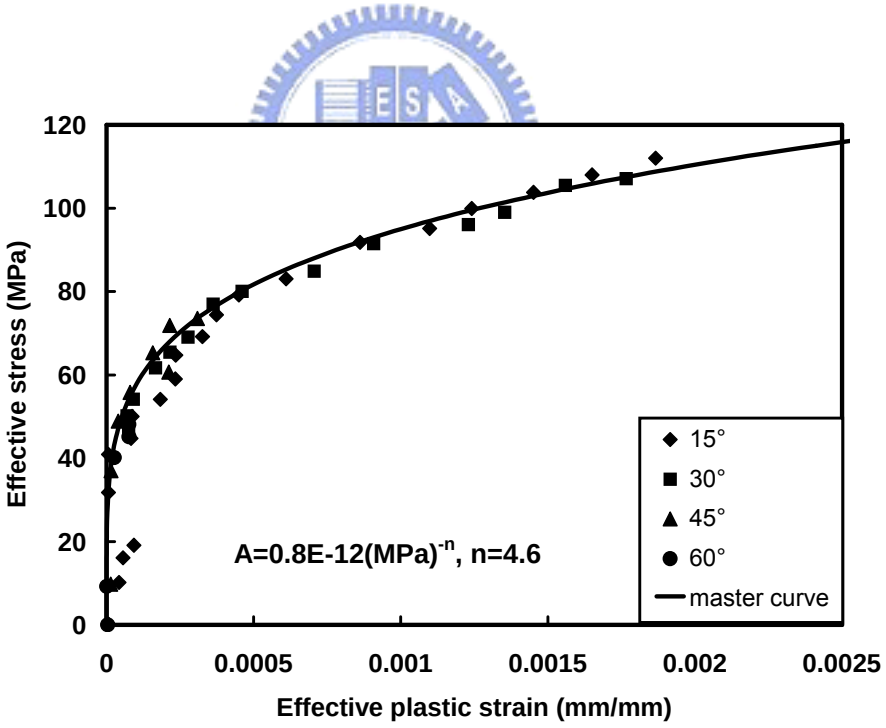

Figure 3.16: Effective stress-effective plastic stain curve for graphite/epoxy at 1/s.

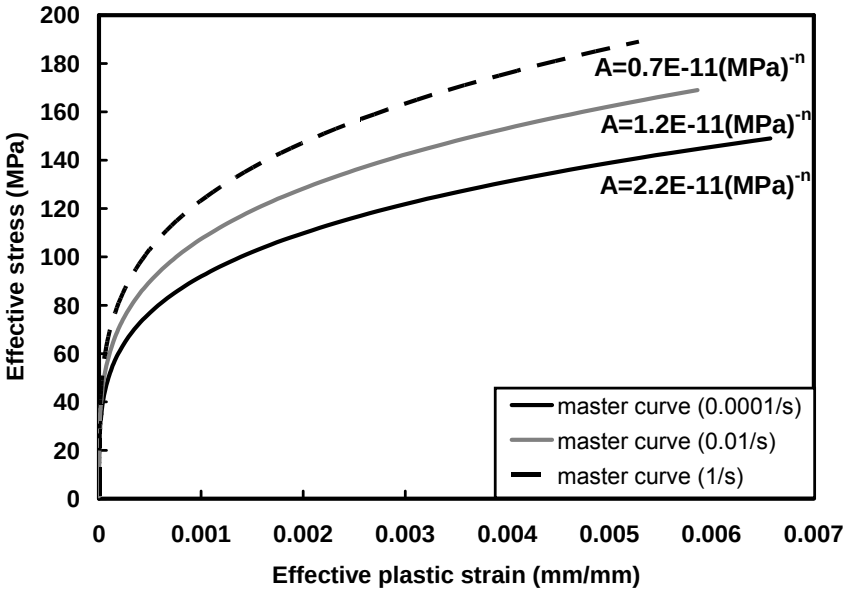

Figure 3.17: Three master curves by power law curve fitted for glass/epoxy.

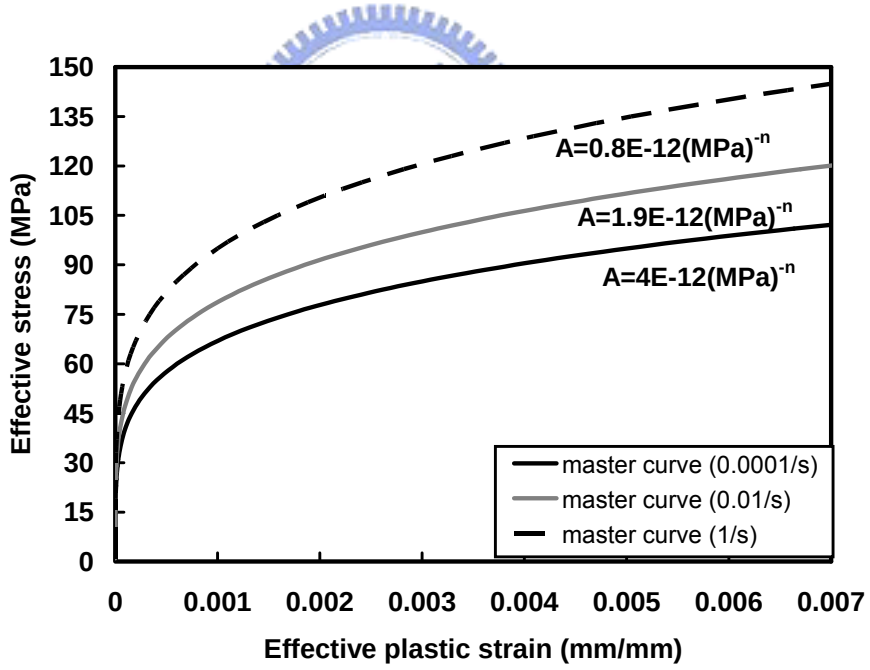

Figure 3.18: Three master curves by power law curve fitted for graphite/epoxy.

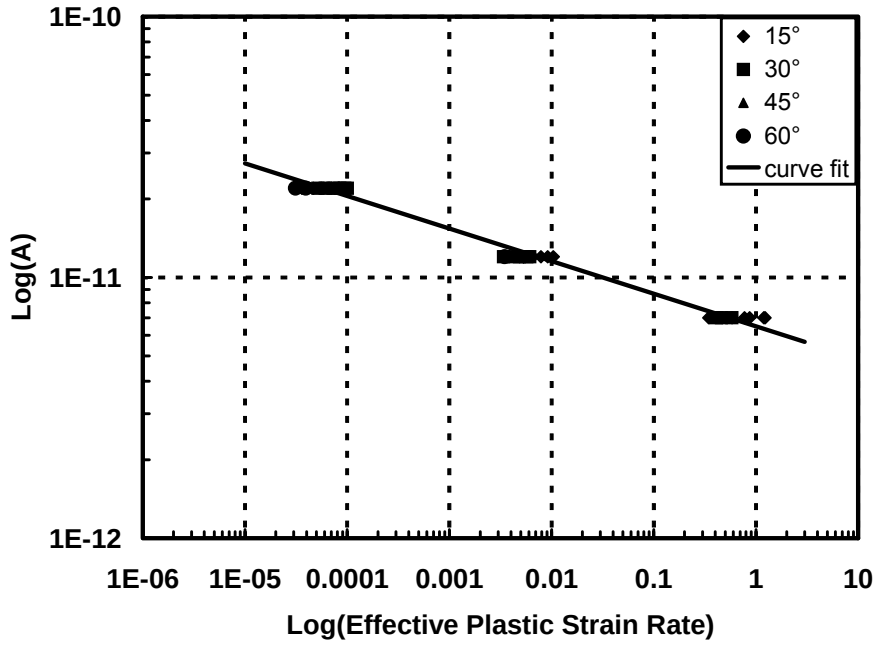

Figure 3.19: The rate dependent amplitude A -effective plastic stain rate relation on a log-log plot for glass/epoxy.

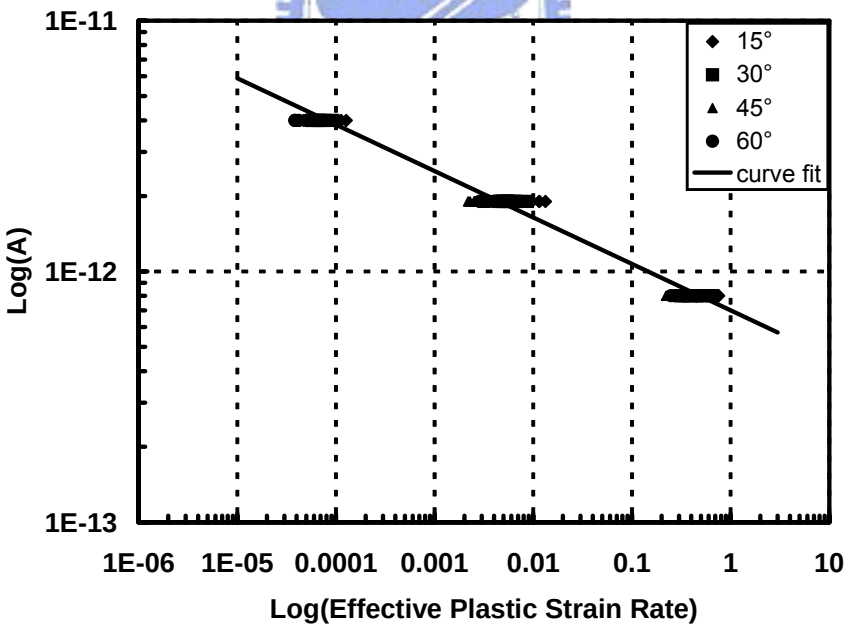

Figure 3.20: The rate dependent amplitude A -effective plastic stain rate relation on a log-log plot for graphite/epoxy.

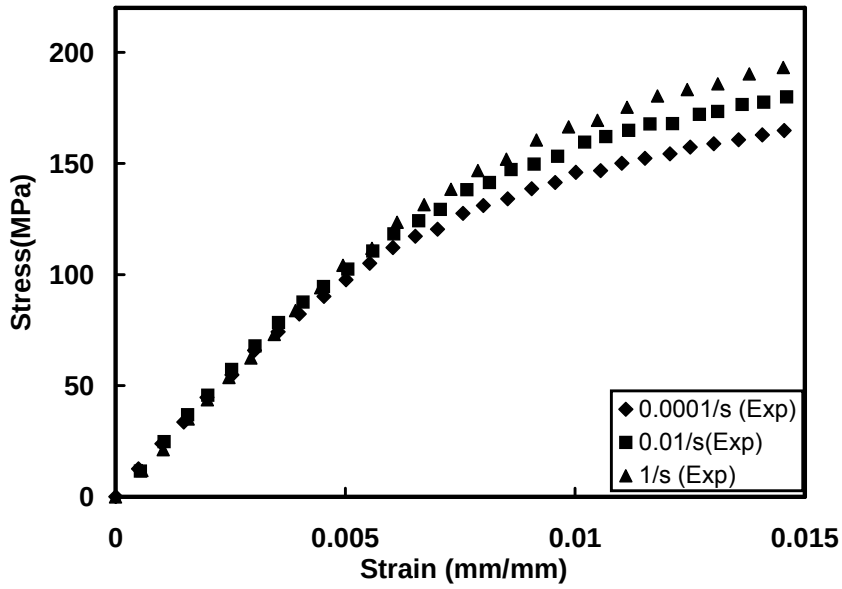

Figure 3.21: Stress and strain curve for $[\pm 45/90_2]_{4s}$ glass/epoxy laminates at various strain rates.

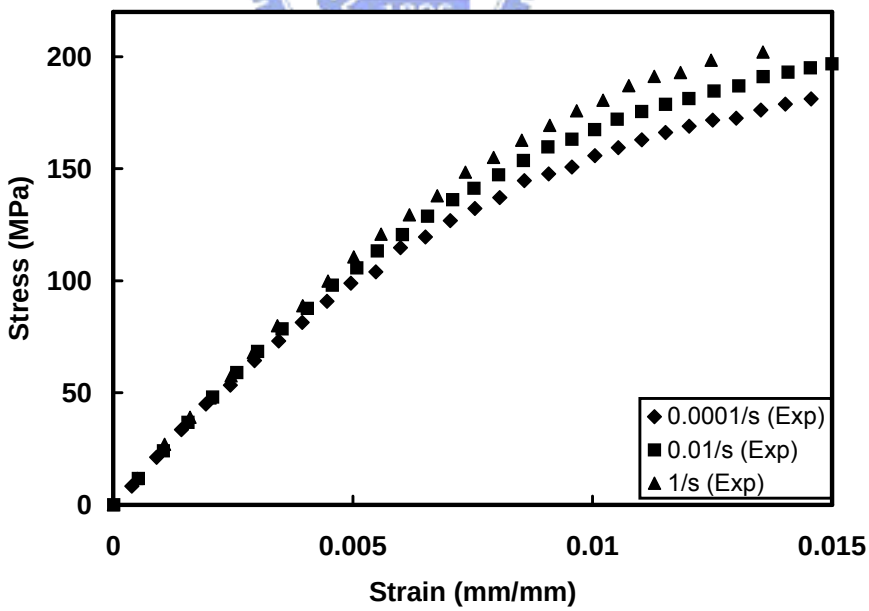

Figure 3.22: Stress and strain curve for $[75_2/-60/30]_{4s}$ glass/epoxy laminates at various strain rates.

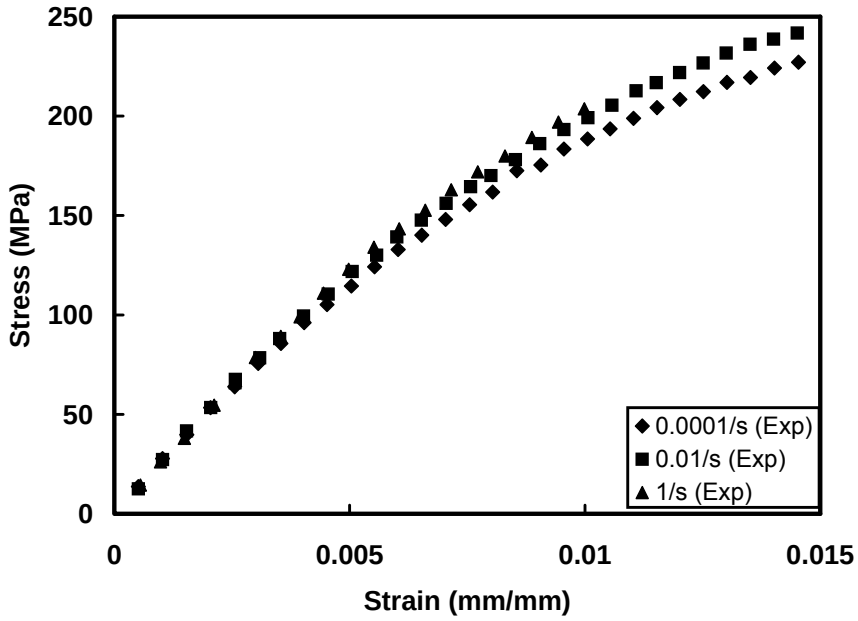

Figure 3.23: Stress and strain curve for $[60_2/-75/15]_{4s}$ glass/epoxy laminates at various strain rates.

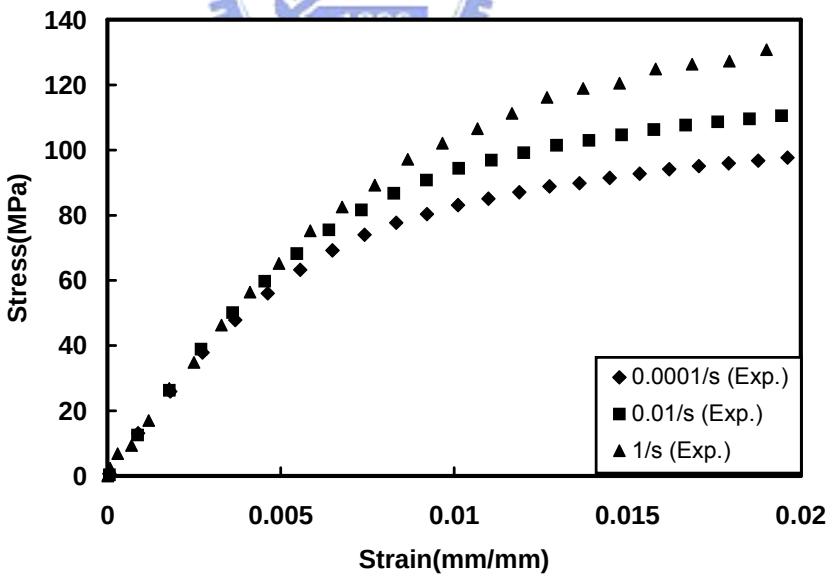

Figure 3.24: Stress and strain curve for $[\pm 45]_{3s}$ graphite/epoxy laminates at various strain rates.

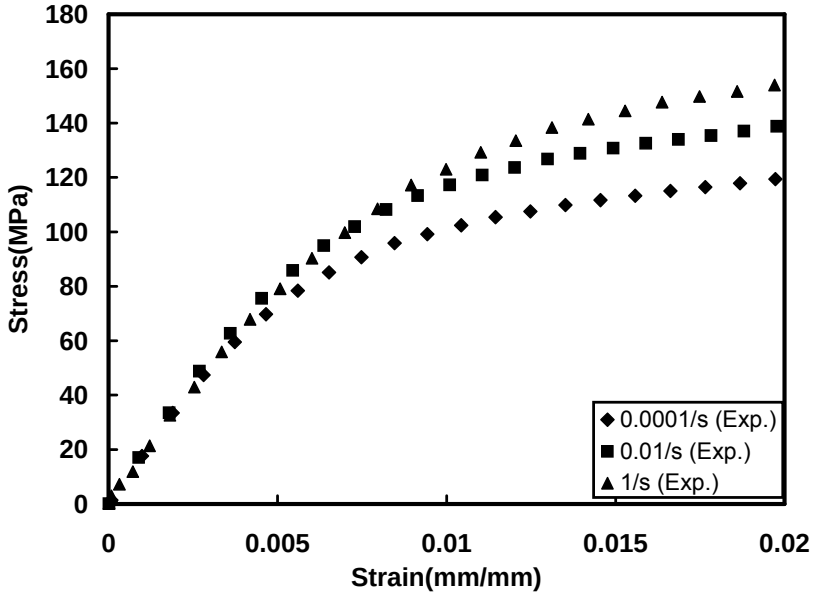

Figure 3.25: Stress and strain curve for $[60/-30]_{3s}$ graphite/epoxy laminates at various strain rates.

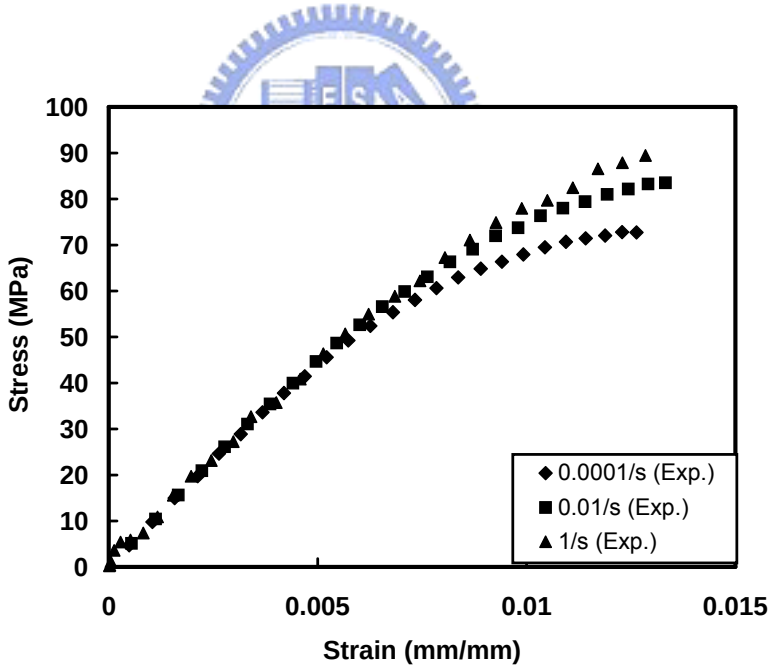

Figure 3.26: Stress and strain curve for $[\pm 60]_{3s}$ graphite/epoxy laminates at various strain rates.

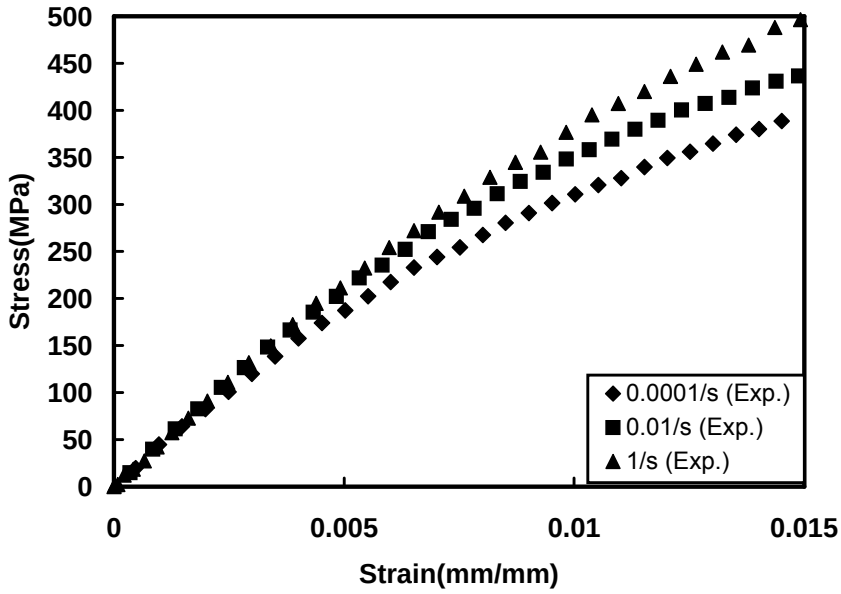

Figure 3.27: Stress and strain curve for $[\pm 30]_{3s}$ graphite/epoxy laminates at various strain rates.

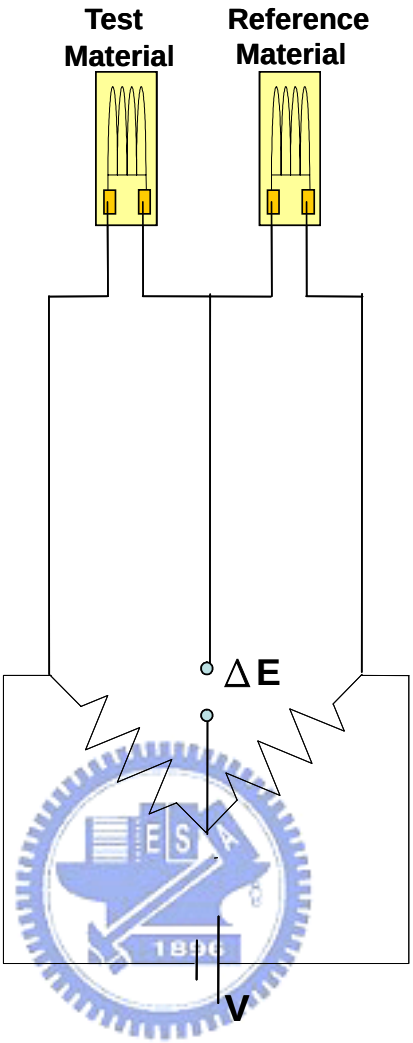

Figure 3.28: Half-bridge circuit for measuring thermal expansion coefficient.

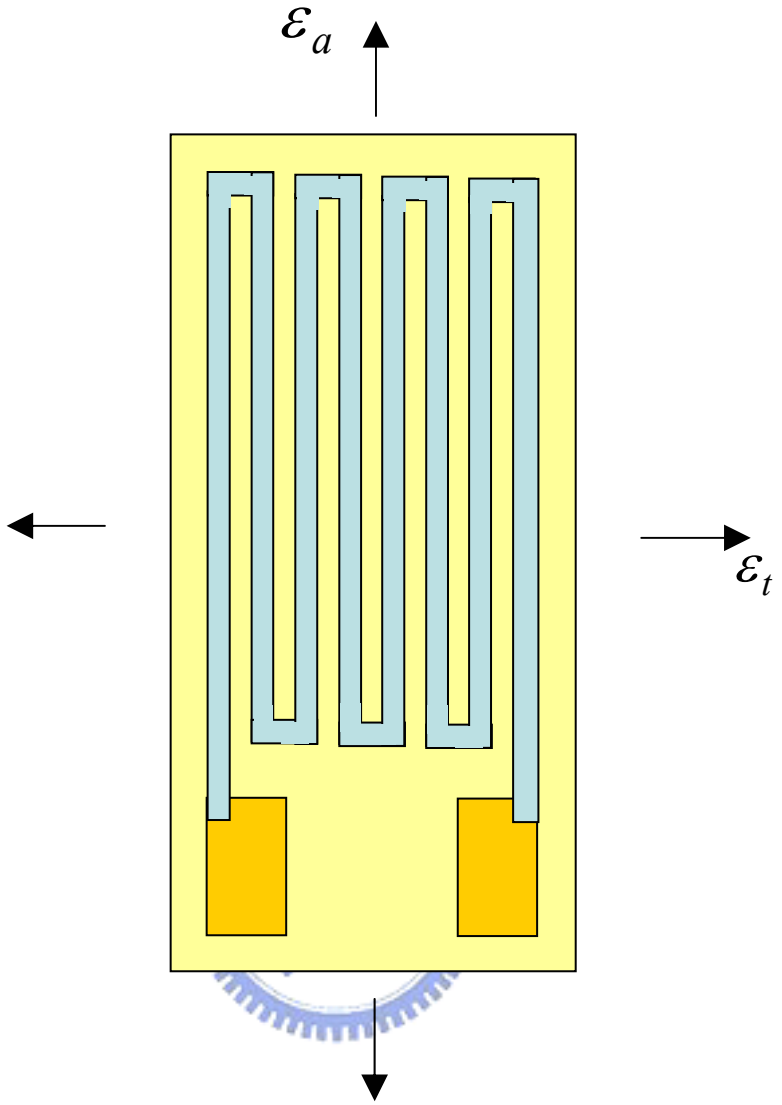

Figure 3.29: Schematic for a strain gage subjected to a biaxial strain field.

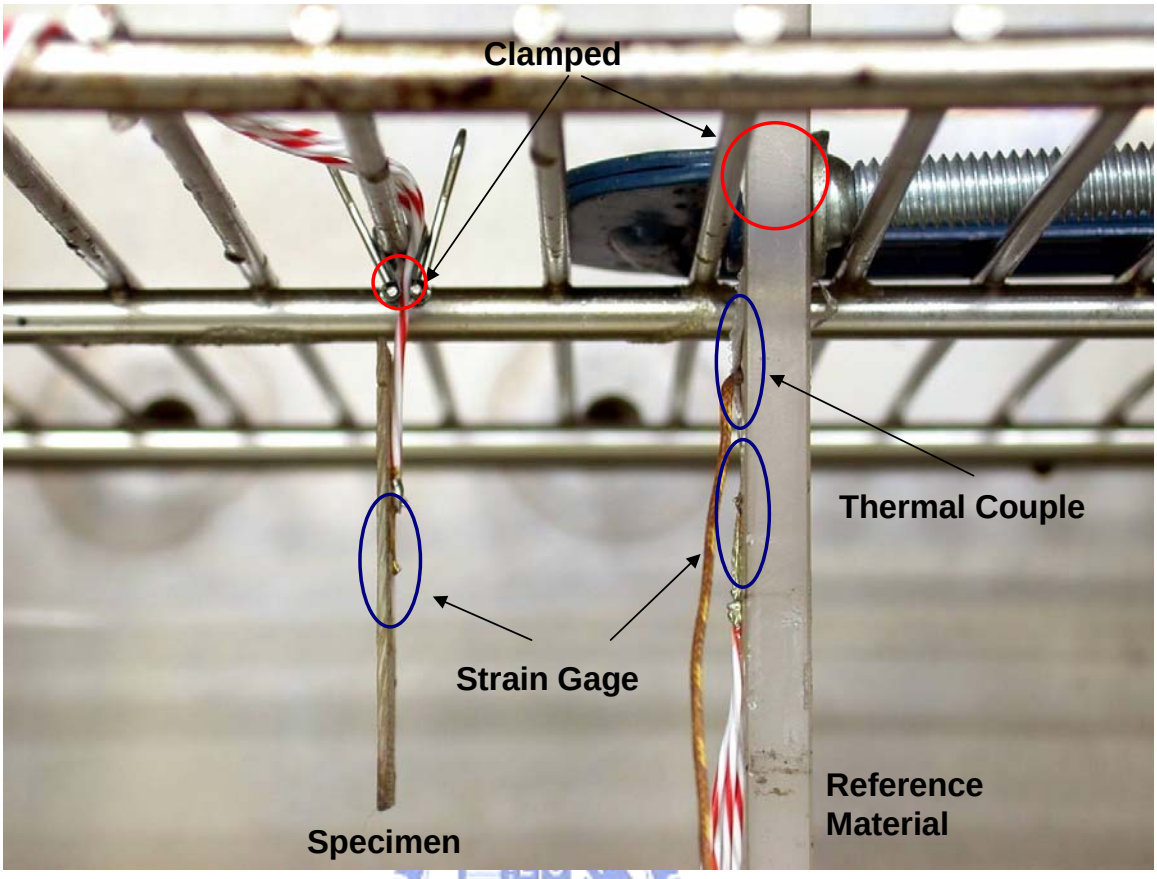

Figure 3.30: Specimen and reference material placed in the oven for measurement.

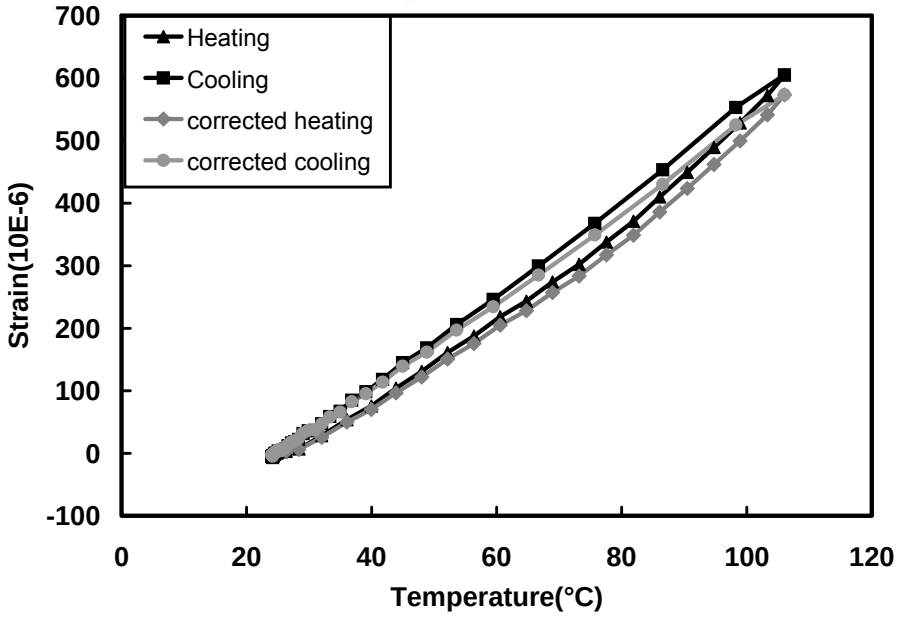

Figure 3.31: Thermal expansion response in the axial direction for glass/epoxy composite.

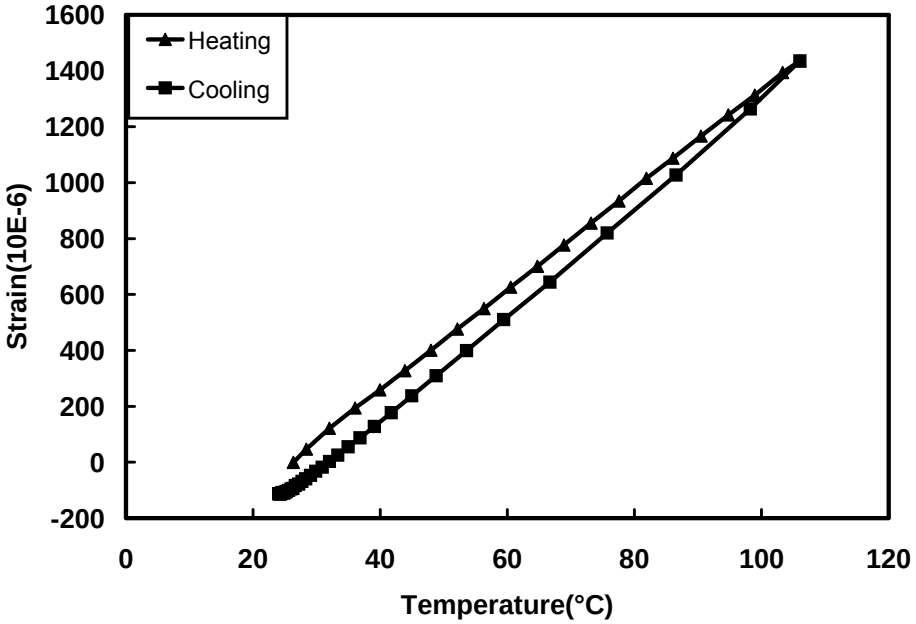

Figure 3.32: Thermal expansion response in the transverse direction for glass/epoxy composite.

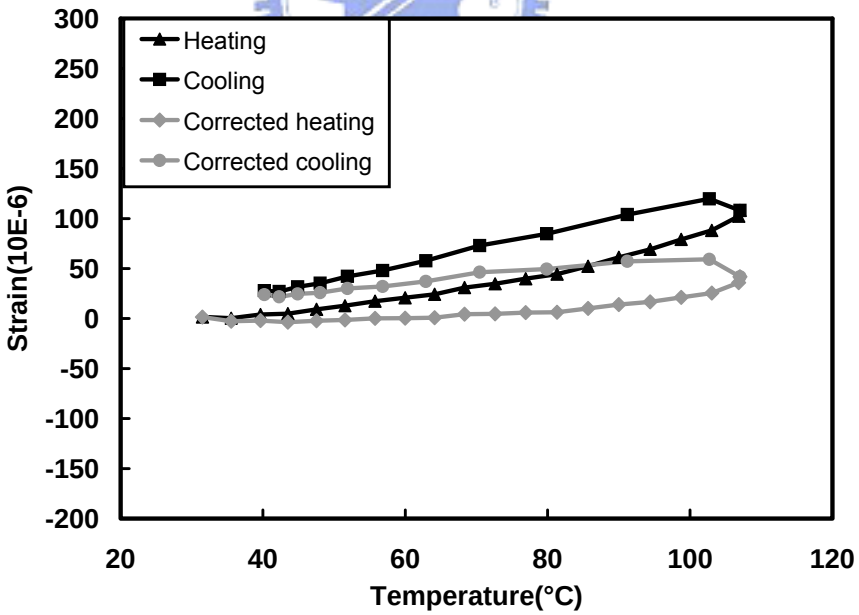

Figure 3.33: Thermal expansion response in the axial direction for graphite/epoxy composite.

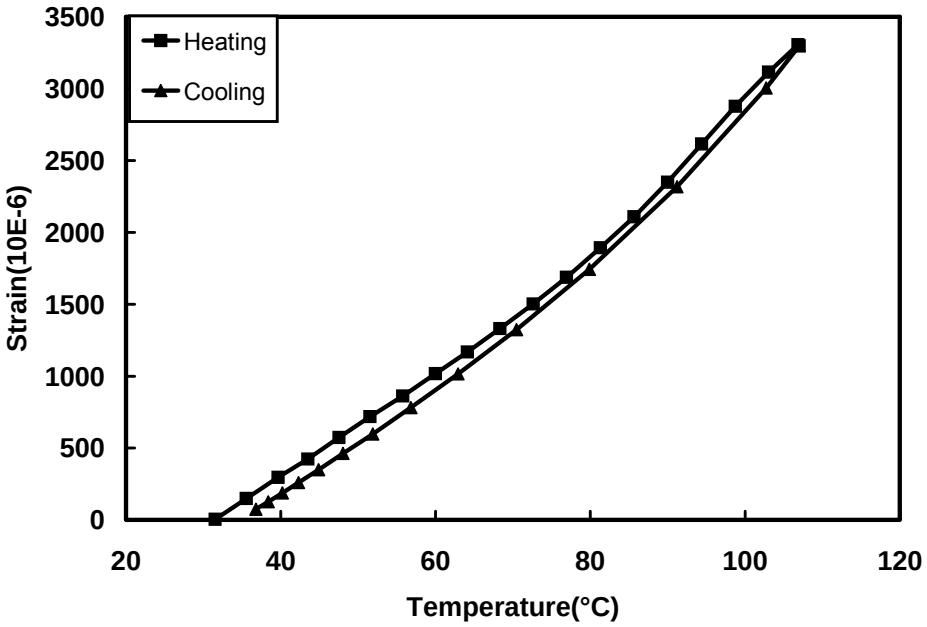

Figure 3.34: Thermal expansion response in the transverse direction for graphite/epoxy composite.

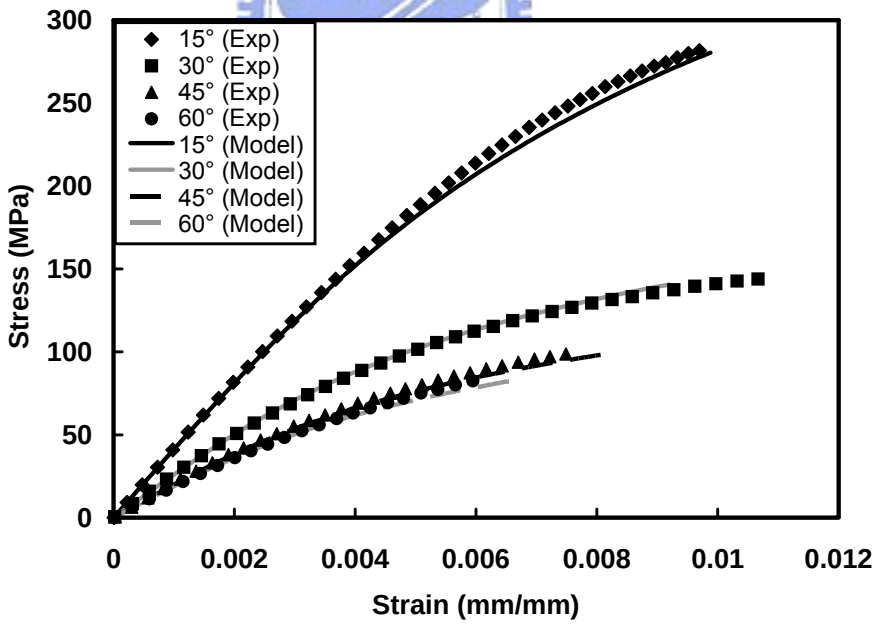

Figure 4.1: Model predictions and experimental results of stress and strain curve for off-axis glass/epoxy composite at strain rate of 0.0001/s.

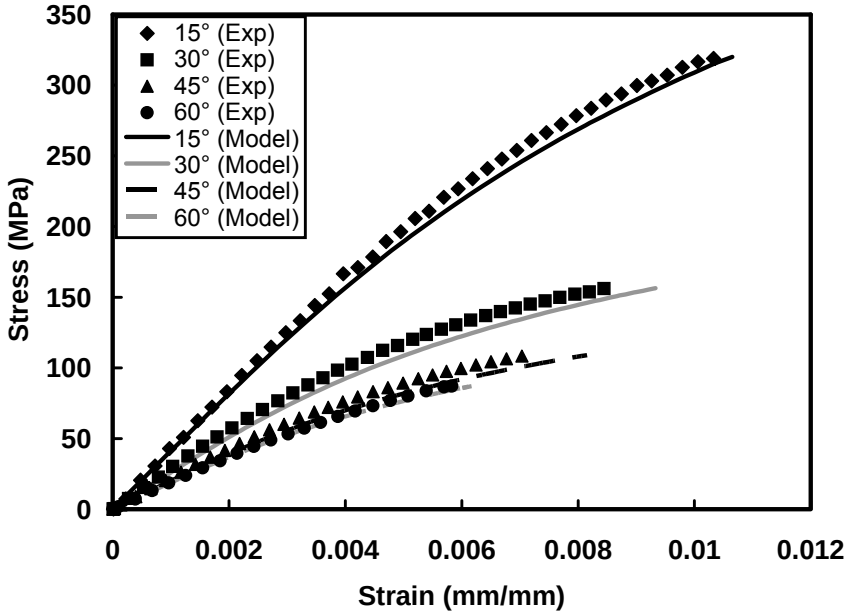

Figure 4.2: Model predictions and experimental results of stress and strain curve for off-axis glass/epoxy composite at strain rate of 0.01/s.

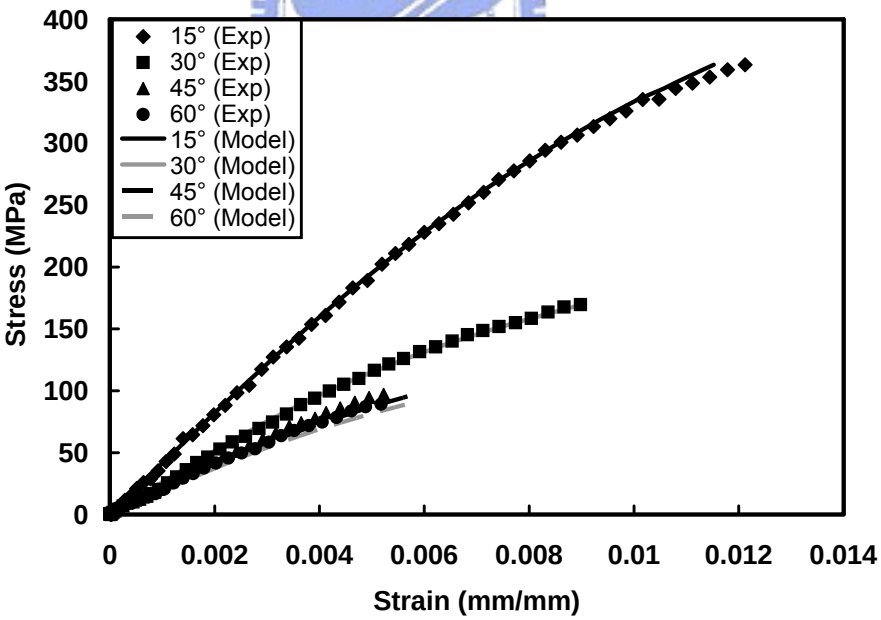

Figure 4.3: Model predictions and experimental results of stress and strain curve for off-axis glass/epoxy composite at strain rate of 1/s.

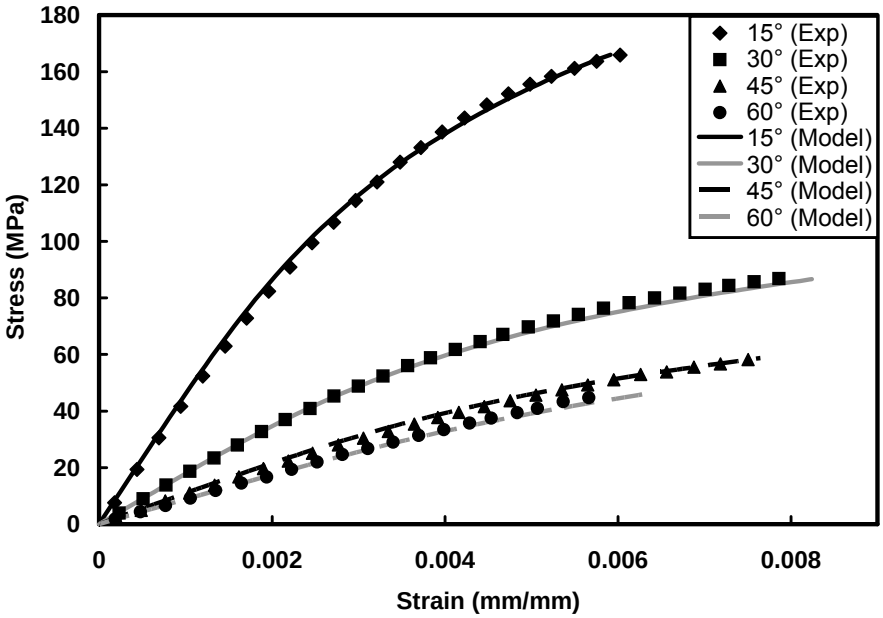

Figure 4.4: Model predictions and experimental results of stress and strain curve for off-axis graphite/epoxy composite at strain rate of 0.0001/s.

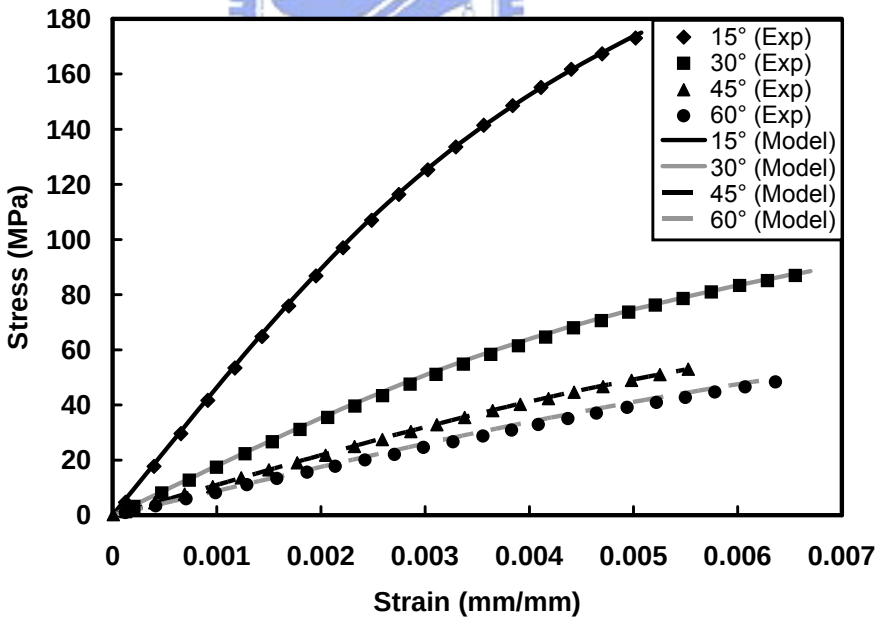

Figure 4.5: Model predictions and experimental results of stress and strain curve for off-axis graphite/epoxy composite at strain rate of 0.01/s.

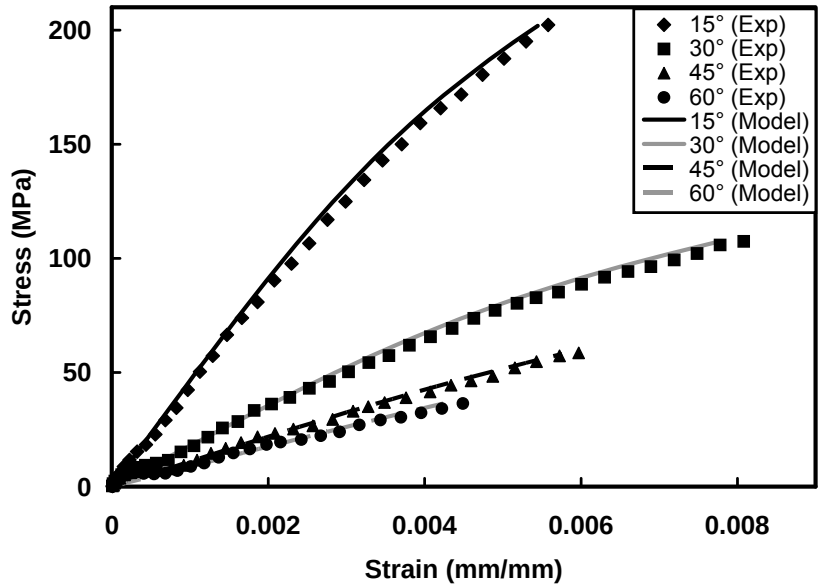

Figure 4.6: Model predictions and experimental results of stress and strain curve for off-axis graphite/epoxy composite at strain rate of 1/s.

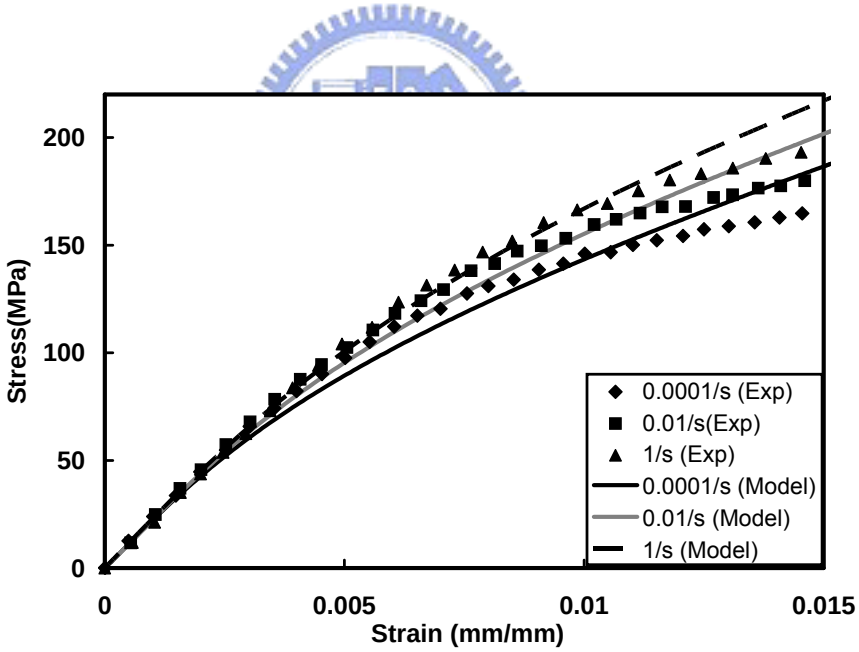

Figure 4.7: Model predictions and experimental results of stress and strain curve for $[\pm 45/90_2]_{4s}$ glass/epoxy laminates at various strain rates.

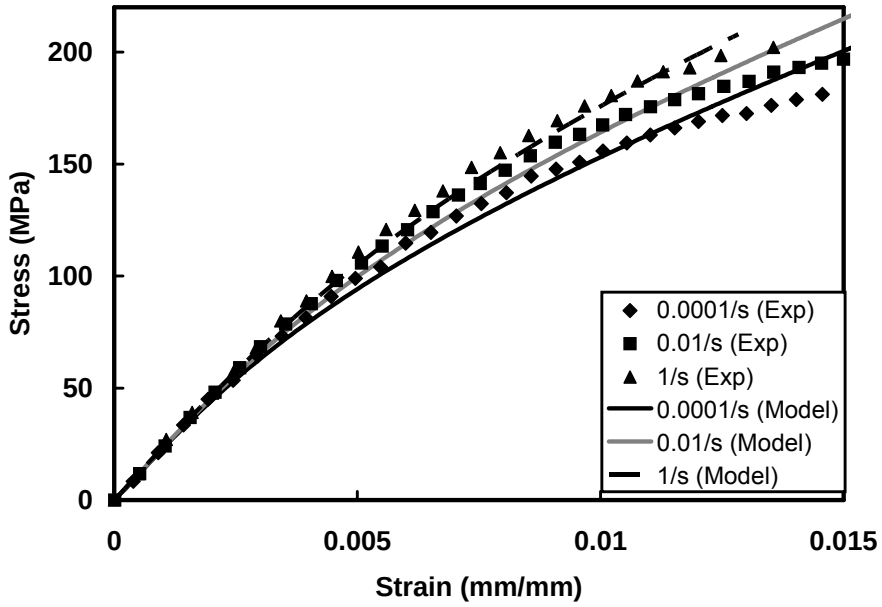

Figure 4.8: Model predictions and experimental results of stress and strain curve for $[75_2/-60/30]_{4s}$ glass/epoxy laminates at various strain rates.

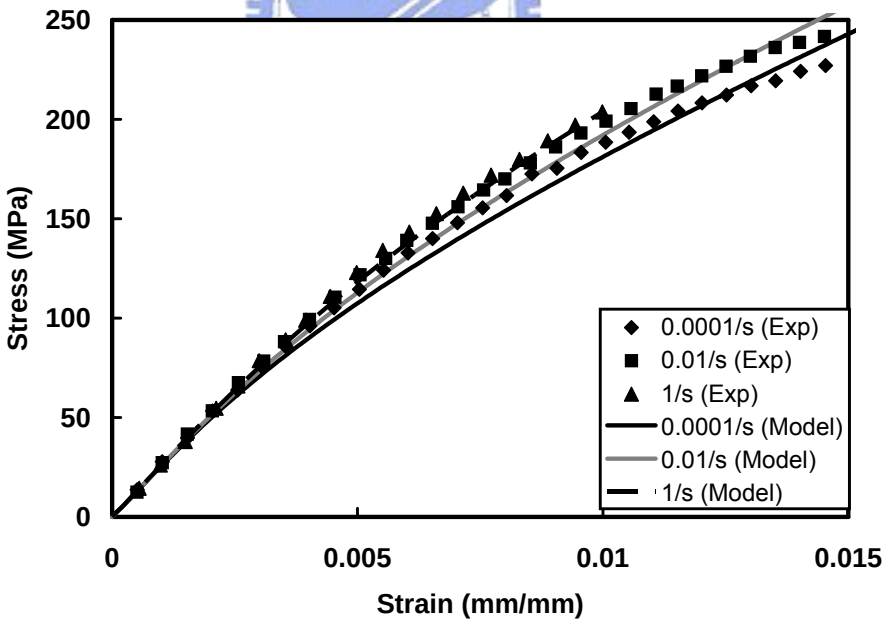

Figure 4.9: Model predictions and experimental results of stress and strain curve for $[60_2/-75/15]_{4s}$ glass/epoxy laminates at various strain rates.

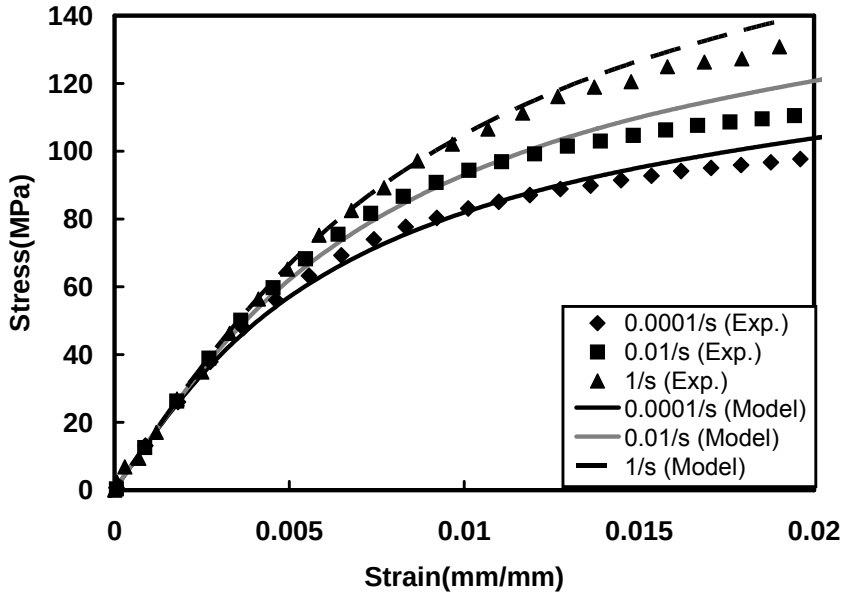

Figure 4.10: Model predictions and experimental results of stress and strain curve for $[\pm 45]_{3s}$ graphite/epoxy laminates at various strain rates.

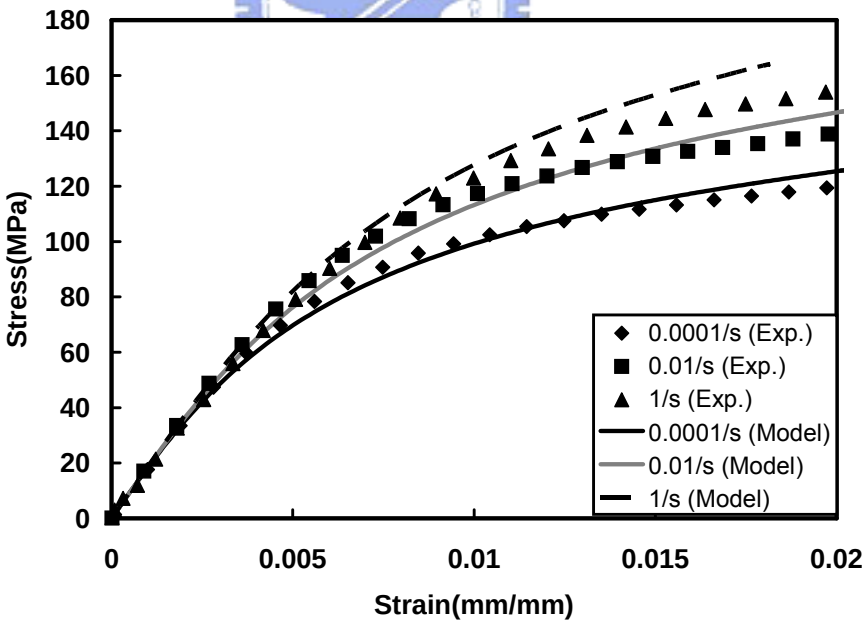

Figure 4.11: Model predictions and experimental results of stress and strain curve for $[60/-30]_{3s}$ graphite/epoxy laminates at various strain rates.

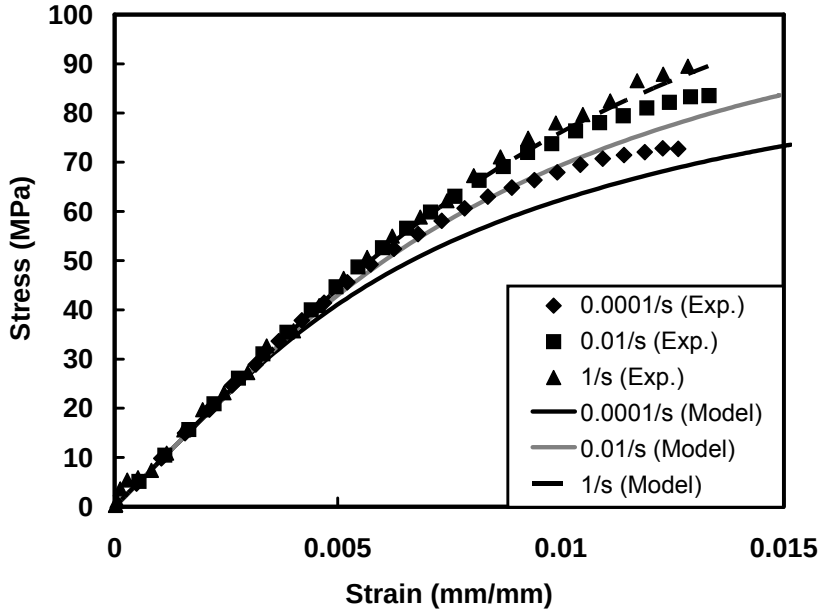

Figure 4.12: Model predictions and experimental results of stress and strain curve for $[\pm 60]_{3s}$ graphite/epoxy laminates at various strain rates.

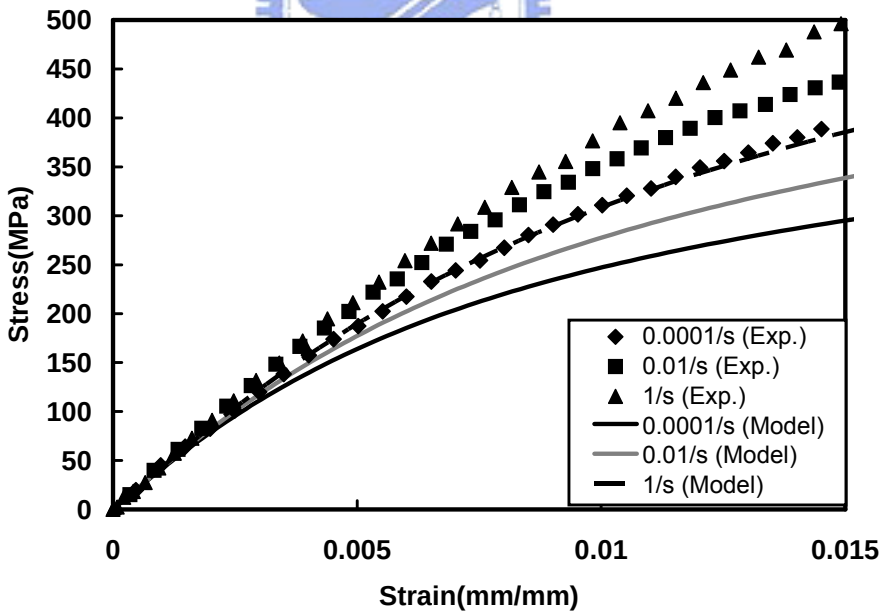

Figure 4.13: Model predictions and experimental results of stress and strain curve for $[\pm 30]_{3s}$ graphite/epoxy laminates at various strain rates.

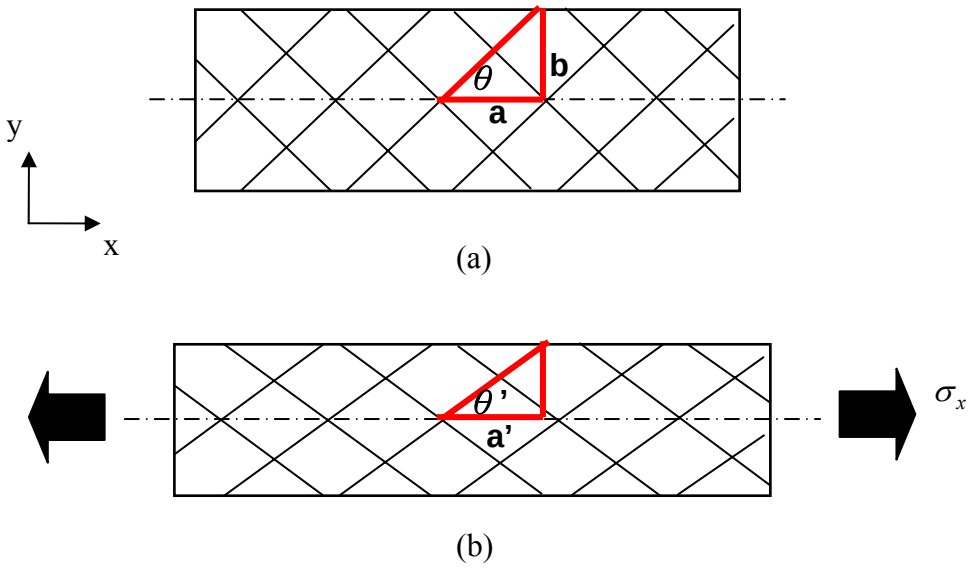

Figure 4.14: Fiber orientation change due to deformation.

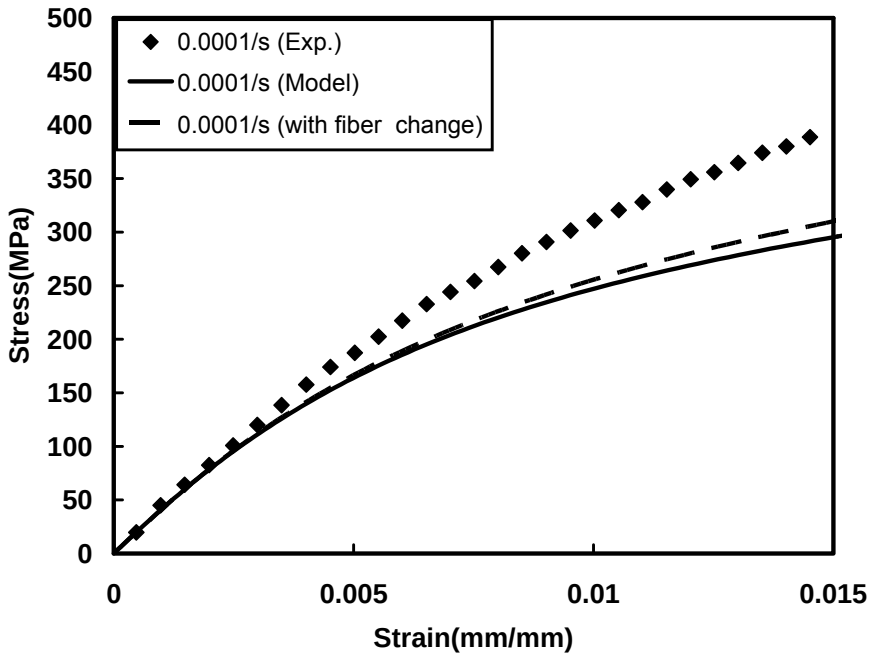

Figure 4.15: Model predictions and experimental results for $[\pm 30]_{3s}$ graphite/epoxy laminates at 0.0001/s. Fiber orientation change was considered.

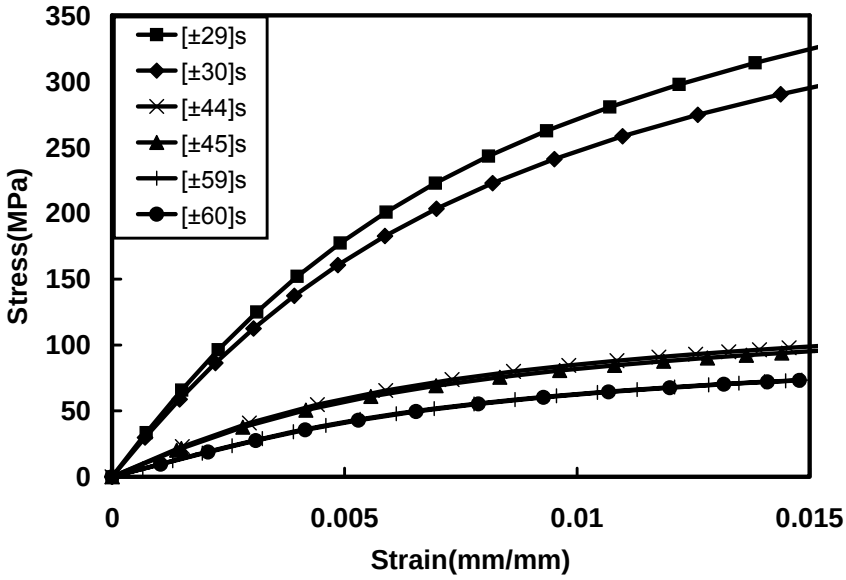

Figure 4.16: Model predictions for $[\pm\theta]_s$ graphite/epoxy laminates at 0.0001/s.

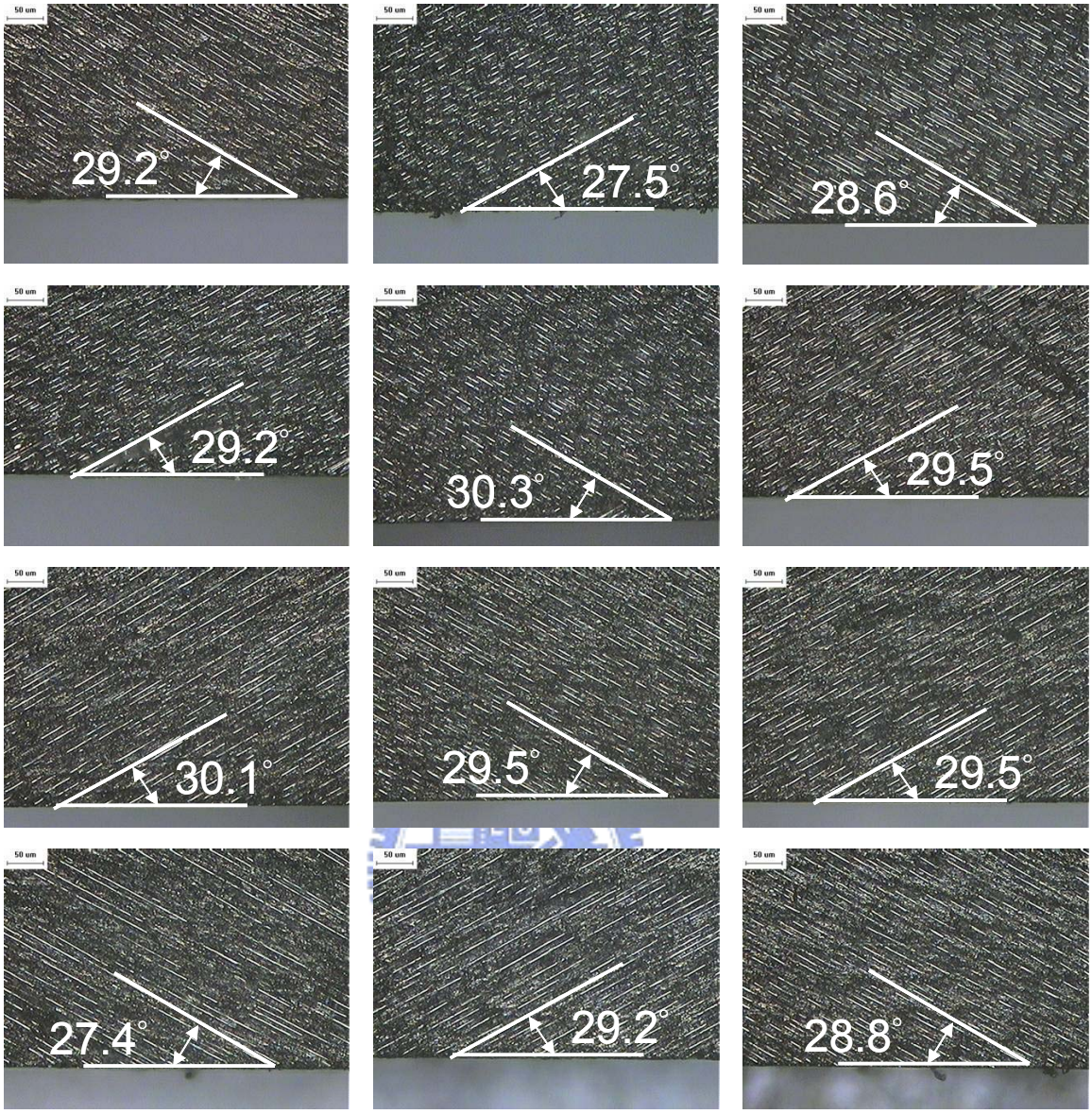

Figure 4.17: Fiber angle of each ply for $[\pm 30]_{3s}$ graphite/epoxy laminate.

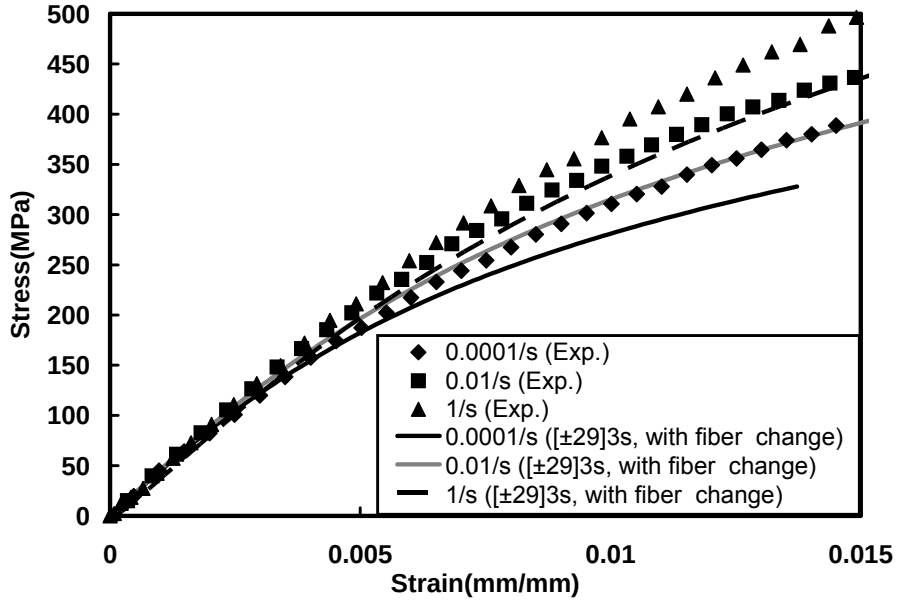

Figure 4.18: New model predictions and experimental results of stress and strain curve for $[\pm 30]_{3s}$ graphite/epoxy laminates at various strain rates. Fiber orientation change was considered.